

A Preliminary Report

BEHAVIOR OF REINFORCED CONCRETE THREE-DIMENSIONAL  
BEAM-COLUMN CONNECTIONS WITH SLABS

by

Kazuhiro Kitayama,  
Shunsuke Otani,  
Hiroyuki Aoyama

April 28, 1986

Department of Architecture  
Faculty of Engineering  
University of Tokyo  
Bunkyo-ku, Tokyo 113  
JAPAN

## INTRODUCTION

The tests of the three-dimensional beam-column connections with slabs were executed as a part of the tri-lateral cooperative research project among the United States, New Zealand and Japan. The main objective of the program is to investigate the behavior of beam-column subassemblages designed in accordance with the building code or standard for reinforced concrete structures of the respective countries. The Japanese specimens were taken from middle floors of an arbitrary proto-type structure, designed in accordance with the Architectural Institute of Japan Standard (AIJ Standard, Ref.1,2), and tested at the University of Tokyo. There is no special provisions for a beam-column connection in the AIJ Standard, and the beam-column connection is normally designed as a non-hinge zone of a column.

The hysteretic behaviour of a beam-column connection is influenced by the bond condition of beam bars within the connection. An improvement in bond of beam bars makes it possible to develop a good spindle-shape hysteresis with flexural yielding at the critical region at beam ends (Ref.3). On the other hand, the bond deterioration of beam bars yields a pinching hysteresis loop attributable to the pull-out of the beam bars from the connection, followed by the shear failure of the connection at a large deformation (Ref.4).

In the past, most of beam-column sub-assemblage tests were carried out on plane beam-column connections, loaded in one horizontal direction. The beam-column connection in an actual structure has both slabs and transverse beams and is subjected to bi-directional loading by earthquake motions. Therefore, it was decided that three-dimensional beam-column connections with slabs be tested in the trilateral program under bi-directional loading. The main variable in the test was chosen to be the bond situation of beam bars within the connection.

## EXPERIMENTAL PROGRAM

Specimens: Three half-scale reinforced concrete three-dimensional beam-column connections with slabs (called K-series) were tested (Table 1); two interior connections (Specimens K1 and K2) and one exterior connection (Specimen K3). The dimensions of the column were varied in the two interior connections; i.e., the column dimensions were 275x275 mm in Specimen K1 and 375x375 mm in Specimen K2. The column dimensions in Specimen K3 were the same as that in Specimen K1. The dimensions of beams were common in the three specimens; 200x300 mm for longitudinal beams (in the primary loading direction) and 200x285 mm for transverse beams. The thickness of slabs was 70 mm. The four corners of the square slab were trimmed to fit into the testing apparatus.

Reinforcement details of the specimens are shown in Fig.1. Beam bars passed through an interior connection, whereas the top and bottom beam bars were anchored within an exterior connection. D13 bars were used as the column reinforcement in the three specimens. The size of the beam bars was varied in the two interior specimens; D13 bars in Specimen K1 and D10 bars in

Specimen K2. D10 bars were used as the beam reinforcement in Specimen K3. The amount of lateral reinforcement (D6 bars) within a connection was decided to be the same as the amount of shear reinforcement of a column in accordance with the AIJ Standard. The slab was reinforced with D6 bars at 180 mm on centers in a single layer, with a 180° hook at each end, but the slab bars in Specimen K3 parallel to the longitudinal beam were anchored in the transverse beams with 90° hooks.

The bond situation of beam bars was made significantly different in the two interior connection specimens by varying the column width and beam bar size. The bond index, defined as an average bond stress of a beam bar within the connection under tensile and compressive yielding assumed at the column faces (Ref. 3), was 102 kgf/cm<sup>2</sup> for Specimen K1 and 57 kgf/cm<sup>2</sup> for Specimen K2 using the actual yield strength of the beam bar. From these index values, the bond of beam bars in Specimen K1 was expected to be quite severe compared to Specimen K2.

The concrete was cast in the upright position in two stages; i.e., the concrete was first placed to the top of the slab, and then cast in the upper column after a day.

Material Properties: The compressive strength of the first batch of the concrete was 244 kgf/cm<sup>2</sup> for Specimens K1 and K2, and 199 kgf/cm<sup>2</sup> for specimen K3. The compressive strength of the second batch was 266 kgf/cm<sup>2</sup> for Specimens K1 and K2, and 196 kgf/cm<sup>2</sup> for Specimen K3.

The yield strength was 4,420 kgf/cm<sup>2</sup> for the D13 bars, 4,460 kgf/cm<sup>2</sup> for the D10 bars, and 4,010 kgf/cm<sup>2</sup> (0.2 % offset) for the D6 bars.

Testing Method: The loading apparatus is shown in Fig.2. The specimens were tested in the upright position. The base of the specimen was supported by a universal joint. The free ends of the beams were supported by vertical rigid members equipped with universal joints at their ends, creating roller support conditions in the horizontal plane. The distance from the column center to the beam-end support was 1,350 mm, and the distance from the beam center to the bottom support or to the top horizontal loading point was 735 mm. The constant vertical load (an average axial stress of 20 kgf/cm<sup>2</sup>) and reversing bi-directional horizontal loads were applied at the top of the column through the tri-directional joint by three actuators. Counter-weights were used to balance the weight of the horizontal actuators. A set of pantograph was attached parallel to the longitudinal beam to prevent a specimen from rotating around the vertical axis.

Loading History: The loading history of Specimens K1 and K2 followed the decision at the Second U.S.-N.Z.-Japan Seminar, Tokyo, 1985 (Ref.5). The story displacement path of the loading point is shown in Fig.3. An ultimate capacity  $P_u$  was calculated at the yielding of the T-shaped beams with 300-mm cooperative slab width on each side. An ultimate state was defined as the state in which the strain at the extreme compression fiber of the concrete reached 0.004. The actual forced story drift history of

the three specimens is shown in Fig.4. The yield drift angle, defined at the Second tri-lateral seminar (Ref.5), was estimated to be  $1/95$  rad for Specimen K3. Therefore, the loading history of Specimen K3 was changed from the agreed displacement history; i.e., the story drift angle of  $1/69$  rad was used instead of two times the yield drift angle.

Instrumentation: The instrumentation system is shown in Fig.5. The deflections of beams and columns relative to the beam-column connection, axial deformation at the top and bottom fiber of beams, beam axial deformation, rotations of beam-end support points around beam axes and connection shear deformation were measured by strain-gauge type displacement transducers. The strain distribution of beam longitudinal reinforcement within and immediately outside the beam-column connection and that of slab reinforcement, the strain of lateral reinforcement within a connection and that of column reinforcement at the critical section were measured by strain gauges. The loads applied by the actuators and beam-end support reactions were measured by load cells.

"Story shear" is defined as the horizontal force corrected for the P-Delta effect, and "story drift angle" as the horizontal displacement of an upper column divided by the distance (= 1,470 mm) from the horizontal load applying point to the bottom hinge of a column.

#### PRELIMINARY CALCULATION

The story shear corresponding to the flexural yielding of a column and beams in the two directions are shown in Fig.6. The ultimate strength of a beam was calculated on the basis of the measured material properties and dimensions with the entire slab as effective in contributing to the beam flexural capacity. When a column is subjected to biaxial lateral loading, the biaxial interaction capacity surface is considered to be a circle. A beam is considered to resist the shear and bending forces only in one direction. Therefore, the capacity surface of a beam is to be two orthogonal lines. From the figure, it is expected that Specimen K1 might develop column yielding immediately after yielding in the beams if loaded in the  $45^\circ$  direction horizontally.

#### TEST RESULTS OF INTERIOR CONNECTIONS

The column reinforcement of Specimen K1 was observed to yield at a story drift angle of  $1/139$  rad during a loading in one direction when the beam reinforcement started to yield. The column reinforcement of Specimen K2 was observed to yield at a story drift angle of  $1/108$  rad during a loading in the two directions after the beam yielding.

Crack Patterns: The crack patterns of the two interior connection specimens K1 and K2 observed at the end of loading are shown in Fig.7.

Specimen K1 developed a single and wide concentrated crack

at the critical section and developed hardly any additional cracks in the beams after a story drift angle of  $1/50$  rad. The shell concrete spalled in the four corners near and within the connection at a story drift angle of  $1/25$  rad.

On the contrary, Specimen K2 developed fine cracks along the beams after a story drift angle of  $1/54$  rad. As expected, the bond situation of beam bars was much improved in the connection from Specimen K1. Cracks were observed more closely in the slab partially because the beams had to deform more in this specimen compared to the stiff columns.

Hysteretic Characteristics: The story shear-story drift relations in the north-south direction are shown in Fig.8. The story drift at yielding was 10.6 mm for Specimen K1 and 6.8 mm for Specimen K2, the difference of which was attributable to the stiffness of the columns.

A story shear resistance in a direction, although the displacement might be maintained in the direction, could be reduced during the loading in the transverse direction due to the biaxial interaction of resistances. Such phenomenon could be observed between points A and B in Fig.8.

Specimens K1 and K2 showed a pinching hysteresis shape under cyclic load reversals. The equivalent viscous damping ratio is used to quantify the fatness of hysteresis loops (Fig.9). The equivalent viscous damping is defined as the hysteretic energy dissipated in each half cycle divided by a triangular area (Fig.10); the part of hysteresis loop under uni-directional loading was used, and the part under bi-directional loading was not used to eliminate the apparent increase in the area due to the biaxial interaction of resistance. The equivalent viscous damping ratio was greater in Specimen K2 than in Specimen K1.

The behavior of a three-dimensional beam-column connection and a plane connection is compared using the specimens with comparable bond index values and subjected to comparable loading. The bond index value was  $57 \text{ kgf/cm}^2$  for Specimen K2, and  $52 \text{ kgf/cm}^2$  for Specimen C2 (a plane beam-column connection specimen tested previously, Ref.3). The equivalent viscous damping ratio was 0.12 for Specimen K2 at a cumulative ductility factor of 35.5 (in the second cycle at a story drift angle of  $1/54$  rad), and 0.21 for Specimen C2 at a cumulative ductility factor of 37.0 (in the fifth cycle at a story drift angle of  $1/46$  rad). Accordingly, the equivalent viscous damping ratio was considerably smaller in Specimen K2 at a comparable story drift angle and cumulative ductility factor. It is likely that the slab might contribute to the pinching in the shape of hysteretic loops.

Generally, such pinching hysteresis shape is observed without bar slip and shear failure when the amount of reinforcement differs significantly at the top and bottom in a beam section. The area of the top beam bars was twice the bottom bars in Specimen C2. In the test of Specimen K2, ten slab bars were observed to have yielded and the remaining two slab bars reached strains above 0.1 % at a story drift angle of  $1/54$ . Therefore, eleven slab bars may well be assumed effective on the

beam resistance. Consequently, the total steel area ( $= 8.51 \text{ cm}^2$ ) of the top beam bars became 2.4 times that of bottom beam bars ( $= 3.57 \text{ cm}^2$ ). The difference may be considered to have influence on the shape of hysteretic loops.

The strain and stress distributions in the top and bottom beam reinforcement of Specimen K2 are shown in Fig.11 at a story drift angle of  $1/216$  rad. The stress was calculated from the strain using the Ramberg-Osgood model for the stress-strain relationship of the steel. A solid line represents the distribution during the loading in the positive direction and a broken line in the negative direction. When the bottom beam bar yielded in tension at an end of a connection, the stress at the other end remained in compression, which indicated a good bond condition of the bottom beam bar within the connection.

On the contrary, the stress in the top bar remained in tension over the entire width of the connection, the stress distribution of which showed a V-shape with a minimum stress appearing near the center. Such stress distribution could not be caused by the bond deterioration. It was thought that the change in the sign of stress in the beam top bar was caused by the rise in the height of the neutral axis above the top beam bar.

Displacement Contribution: The contribution of parts of a specimen to the story drift was calculated and shown in Fig.12. The contribution of the beam-column connection panel deformation was calculated as the total deflection less the contribution from the beam and column deflections. The deflection of beams for Specimen K2 shares 80 % of the total story drift in contrast to 60 % for Specimen K1. The difference of the beam contribution was caused by the difference in the stiffness of a column. The deformations of the connection and column are considered to have much influence upon a hysteretic behavior in Specimen K1.

The contribution of local rotation in various regions along a beam to the beam deflection was calculated and shown in Fig.13. The rotation was measured over a  $D/6$  distance from a column face, and over successive  $D/3$ ,  $D/2$  and  $D$  distances, where  $D$  is a beam overall depth ( $=300 \text{ mm}$ ). The four regions are called Region 1 to Region 4 from the column face. The rotation in Region 1 was caused mainly by the pull-out of beam bars from the connection. The deflection component of Region 1 of Specimen K1 reached 70 % of the total beam deflection at a beam deflection of 20 mm, indicating a large pull-out of beam bars from the connection. On the other hand, the deflection component of Region 1 of Specimen K2 was 50 % of the total beam deflection at the same deflection level.

Stress Distribution of Slab Bars: The stress distribution of slab reinforcement parallel to the longitudinal beam and at the face of the transverse beams is shown in Fig.14 at peaks of loading cycles. Stress was calculated from strain by the Ramberg-Osgood model. The stresses under negative bending (the top fiber in tension) increased toward the longitudinal beam, and with a story drift. The slab bars which were apart from the longitudinal beam showed a tensile stress even under positive bending (top

fiber in compression). This was considered to be caused by the transverse beams subjected to torsion and a deformation within a horizontal plane (Ref.5).

#### TEST RESULTS OF AN EXTERIOR CONNECTION

The column was observed to yield at a story drift angle of  $1/69$  rad during a bi-directional loading one loading cycle after the beam yielding.

Crack Pattern: The crack pattern observed at the end of loading is shown in Fig.15. Torsional cracks were observed in the transverse beams near the column during the loading in the longitudinal direction. But its width was small so that the transverse beams did not fail in torsion. Diagonal shear cracks were observed in the connection panel region in the transverse direction. During loading in the transverse direction, cracks in the slab were almost parallel to the longitudinal beam and didn't incline toward  $45^\circ$  as seen during loading in the longitudinal direction. Note that the one-sided slab influenced a crack pattern of the slab.

Hysteretic Characteristics: The story shear-story drift relation in the longitudinal direction is shown in Fig.16 with the calculated restoring force characteristics with different effective widths of the slab. The widths of the slab were (a) the entire slab width (total width B of T-section=239 cm), (b) the cooperating width specified by the AIJ Standard (B=74 cm) and (c) zero (B=20 cm). Within a range of small story drift, the stiffness was observed similar to the one calculated with no slab width. The resistance at a story drift angle of  $1/69$  rad was observed almost equal to the value calculated with the entire slab width.

Stress Distribution of Slab Bars: The stress distributions of slab reinforcement in the two directions are shown in Fig.17 at peaks of each loading cycle. Solid and broken lines represent the distribution when the top of a beam section is subjected to compression and tension, respectively. In the transverse direction, the slab bars passing through the longitudinal beam had a tensile stress at the face of the longitudinal beam even in the negative bending (top fiber in compression). On the other hand, the slab bars in the longitudinal direction near a column were subjected to compression at the peaks under positive bending (top fiber in compression) and the number of compressed slab bars increased with the amplitude of story drift angle. But the slab bars away from the column developed tensile stress.

If the effective width of a slab is determined by the number of yielded slab bars, not much difference was observed in the longitudinal and transverse directions. In both directions, all slab bars yielded beyond a story drift angle of  $1/25$  rad.

If a slab locates only on one side of beams and the torsional resistance of the transverse beam is sufficient to take the reaction of tensile forces resulted from the slab bars, the entire slab width is regarded as effective at a large story drift

angle. The transverse beams could fail in torsion when the introduced torsional force increases with an amount of slab bars.

Behavior of Transverse Beams and Slab: The horizontal deflection of the transverse beams is shown in Fig.18 at a story drift angle of 1/188 rad during the loading in the longitudinal direction. The transverse beams scarcely showed a horizontal deflection when the top of the longitudinal beam was compressed. But when the top fiber of the longitudinal beam was subjected to tensile stress, the transverse beams deflected in the horizontal plane by the tensile force exerted by the slab bars. This horizontal deflection was 3 or 4 times larger than that of the interior connection specimens.

Strain distribution of slab bars in the two directions is shown in Fig.19 at a story drift angle of approximately 1/120 rad. When the story shear was applied only in the longitudinal direction, the slab bars away from the column and parallel to the transverse beam showed tensile strain (locations E and F in Fig.19). On the contrary, during loading only in the transverse direction, the slab bars away from the column (locations K and L) indicated no strain and the slab bars near the column (locations G, H and I) developed tensile strains.

#### EFFECT OF BEAM BAR BOND ON HYSTERETIC SHAPE

One of the objectives in this test was to study the effect of bond situation of beam bars on a hysteretic behavior of a three-dimensional beam-column connection with slabs. Beam bar bond index  $u_b$  (Ref.3), an index proposed to indicate the bond situation of beam bars in a connection, was used to design the specimens on the basis of the test results on the plane frame connections.

The beam bar bond index  $u_b$  was defined as follows :

$$u_b = f_y \cdot (d_b/h_c) / 2$$

where  $f_y$  : yield strength of a beam bar,  $d_b$  : diameter of a beam bar and  $h_c$  : column width. The amplitude of index  $u_b$  depends on both column depth-to-beam bar diameter ratio and the yield strength of a beam bar.

The results of twelve plane beam-column subassemblages (Refs.3 and 4), were studied with regard to a hysteretic shape and the beam bar bond index. The twelve specimens developed a beam-yielding prior to failure. Nine specimens resulted in a pinching behavior and the rest showed a good-spindle shape behavior. An equivalent viscous damping ratio was used as the index to represent the fatness of a hysteretic loop. The beam bar bond index and an equivalent viscous damping ratio relations of twelve specimens are shown in Fig.20. The actual yield strength was used in calculating the index value. The equivalent viscous damping ratio was evaluated in the second cycle at a story drift angle of 1/46 rad using the peak resistance and deflection in the second cycle. Points plotted in this figure are distributed within a linear band which inclines right-downwards. The beam bar



bond index may be used to indicate a bond situation of beam bars within a connection.

#### CONCLUDING REMARKS

From the test results, the following conclusions were drawn;

1) The interior beam-column subassemblage with slabs, designed to improve the bond of beam bars within a connection taking into account the beam bar bond index showed a pinching behavior. The bond of beam bars within a connection was considered to be good judging from the strain distribution of beam bars. It is considered that the pinching behavior was caused by the delay of crack closing due to the difference in the amount of effective beam top and bottom reinforcing bars.

2) For an exterior beam-column subassemblage with slabs only on one side, the width of the slab effective to the beam resistance spread with the beam deflection. The entire slab width needs be regarded as effective if the torsional resistance of a transverse beam is sufficient to prevent the failure by torsion.

#### ACKNOWLEDGEMENTS

The experimental work reported in this paper was carried by K. Kitayama as a part of a master of engineering study at the University of Tokyo. Mr. S. Asami assisted the test toward his bachelor of engineering thesis, University of Tokyo. The authors are grateful to the assistance provided by Messrs. Y. Hosokawa and A. Tasai, research associates in Department of Architecture, and the members of Aoyama Laboratory, University of Tokyo, in executing the experimental work.

#### REFERENCES

1. Architectural Institute of Japan, "AIJ Standard for Structural Calculation of Reinforced Concrete Structures (in Japanese)", revised in 1982.

2. Aoyama, H., K. Kitayama, and S. Otani, "Design of Reinforced Concrete Beam-Column-slab Specimens in Accordance with Japanese Practices", A Paper presented during U.S.-New Zealand-Japan Seminar on Design of Reinforced Concrete Beam-Column Joints, Tokyo, May 28 and 29, 1985.

3. Otani, S., K. Kitayama, and H. Aoyama, "Beam Bar Bond Stress and Behavior of Reinforced Concrete Interior Beam-Column Connections", Report prepared for U.S.-N.Z.-Japan Seminar, Tokyo, May, 1985.

4. Otani, S., Y. Kobayashi, and H. Aoyama, "Reinforced Concrete Interior Beam-Column Joints under Simulated Earthquake Loading", A paper presented during the U.S.-New Zealand-Japan Seminar on Design of Reinforced Concrete Beam-Column Joints, Monterey, California, July 30-August 1, 1984.

5. Minutes of trilateral meeting in Tokyo, 1985.

6. Suzuki, N., S. Otani, and Y. Kobayashi, "Three-Dimensional Beam-Column Subassemblages Under Bidirectional Earthquake Loadings", Proceedings, Eighth World Conference on Earthquake Engineering, San Francisco, July, 1984.

Table 1: Properties of K-Series Specimens

Specimen	K1	K2	K3
(a) Longitudinal Beam			
Top Bars	4-D13	7-D10	7-D10
$a_t(\text{cm}^2)$	5.08	4.99	4.99
$p_t(\%)$	1.00	1.01	1.01
Bot. Bars	3-D13	5-D10	5-D10
$a_t(\text{cm}^2)$	3.81	3.57	3.57
$p_t(\%)$	0.71	0.66	0.66
Stirrups	2-D6	2-D6	2-D6
@ (cm)	5.0	5.0	5.0
$p_w(\%)$	0.64	0.64	0.64
(b) Column			
Total Bars	16-D13	12-D13	16-D13
$a_g(\text{cm}^2)$	20.32	15.24	20.32
$p_g(\%)$	2.69	1.08	2.69
Hoops	4-D6	2-D6	4-D6
@ (cm)	5.0	5.0	5.0
$p_w(\%)$	0.93	0.34	0.93
Load(tonf)	15.1	28.1	15.1
(kgf/cm <sup>2</sup> )	20.0	20.0	20.0
(c) Slab			
Total Bars	12-D6	12-D6	12-D6
st.ratio(%)	0.23	0.23	0.23
(d) Connection			
Hoops	2-D6	2-D6	2-D6
sets	4	4	3
$a_w(\text{cm}^2)$	2.56	2.56	1.92
$p_w(\%)$	0.42	0.33	0.34

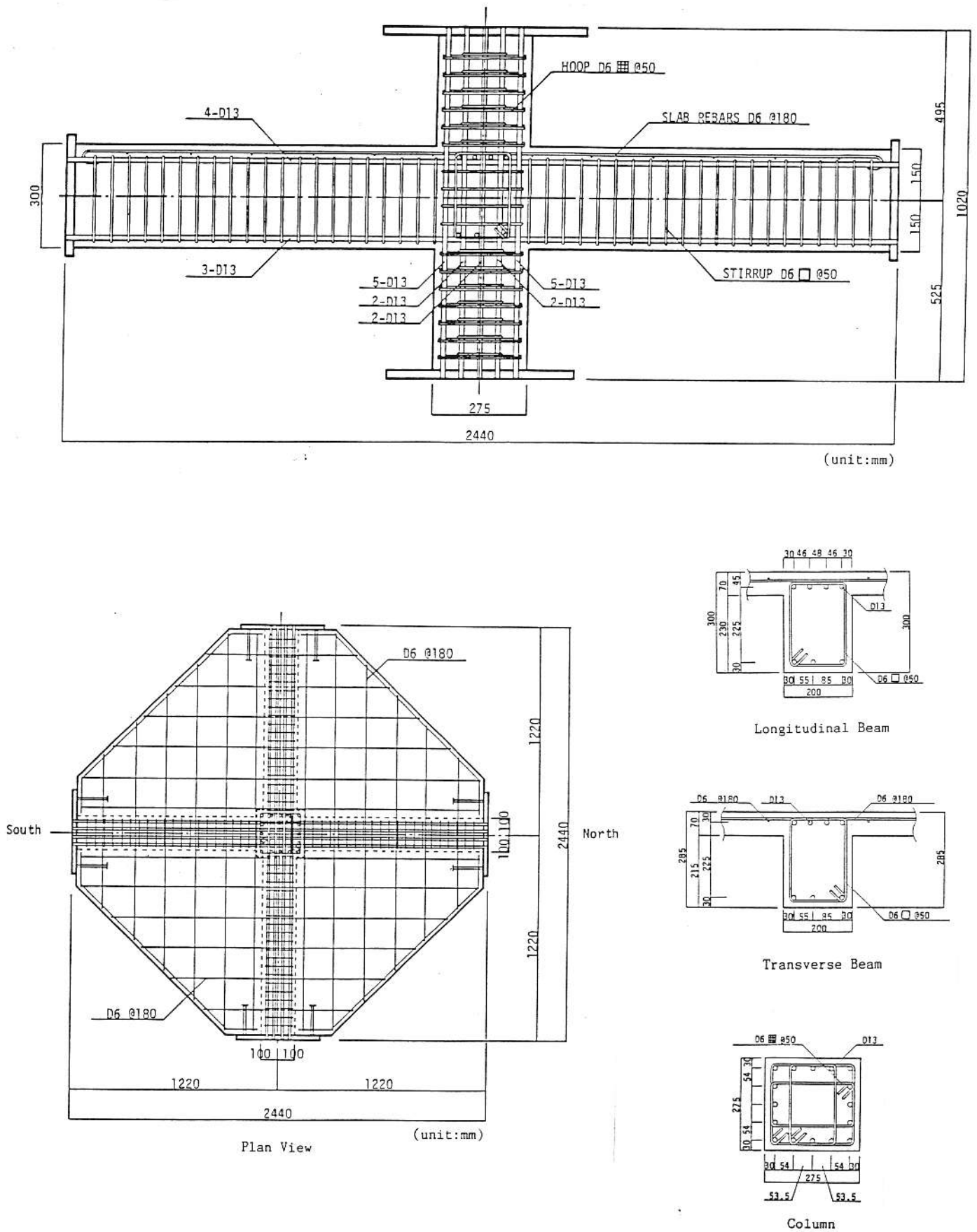


Fig.1: Reinforcement Details of Specimen K1

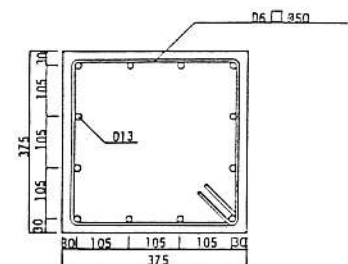
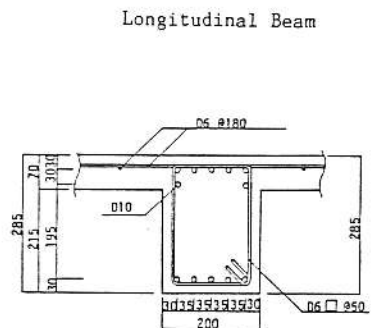
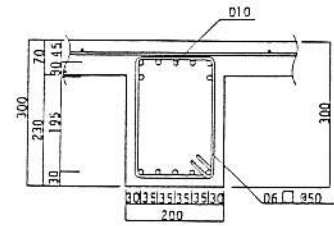
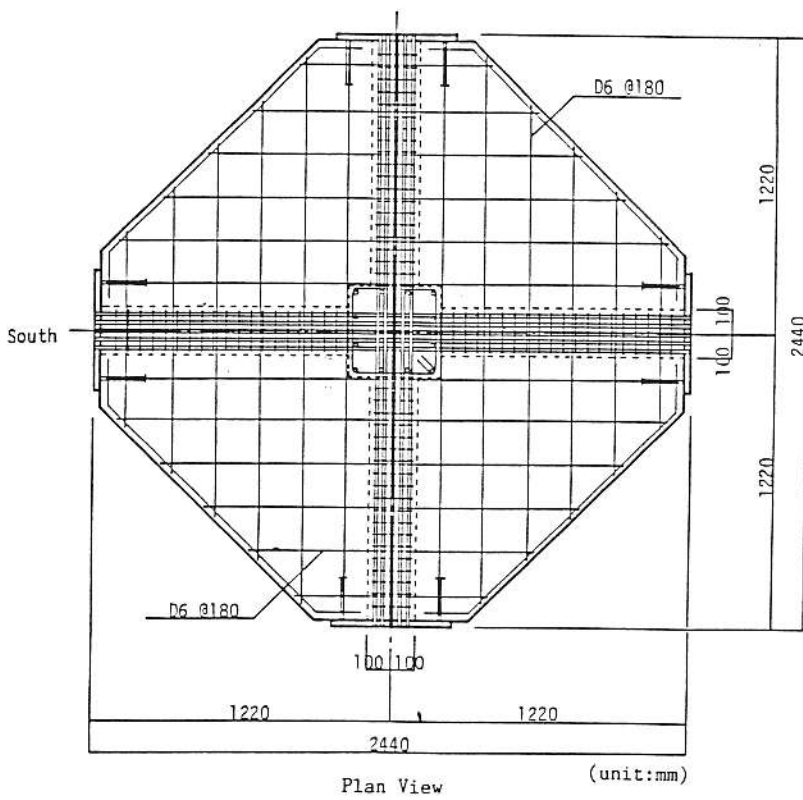
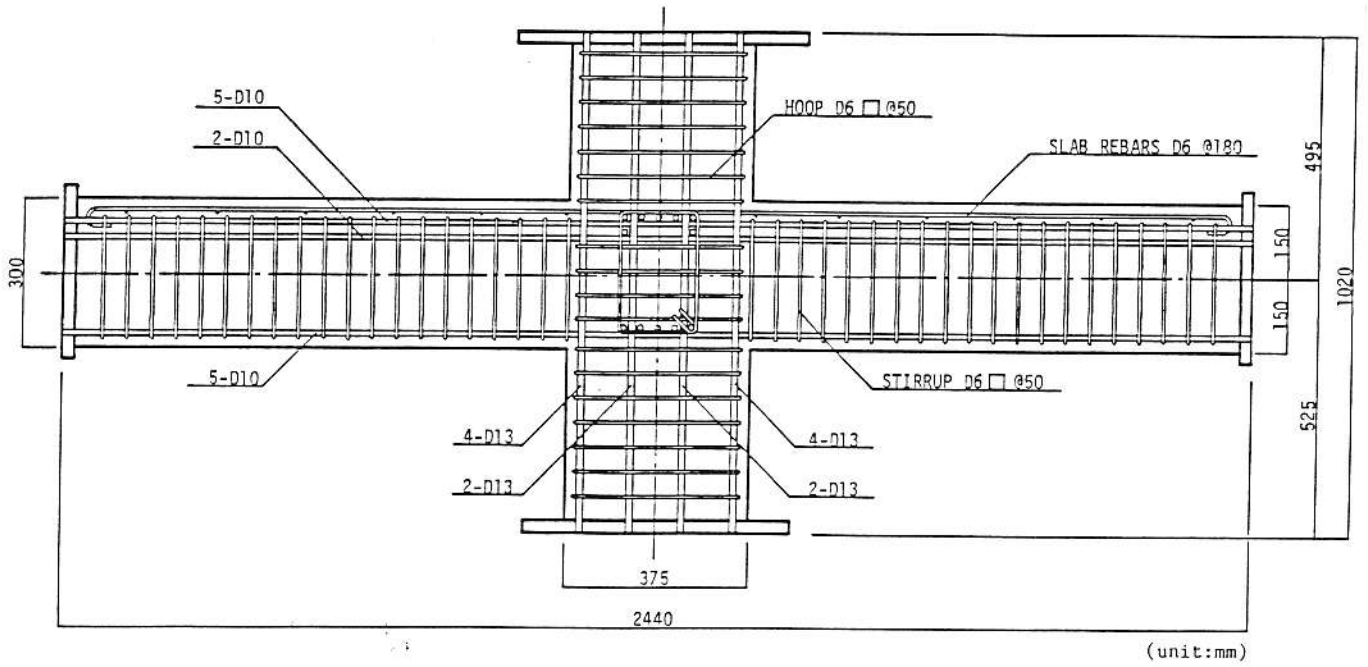
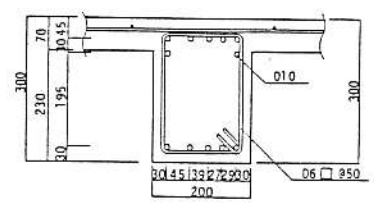
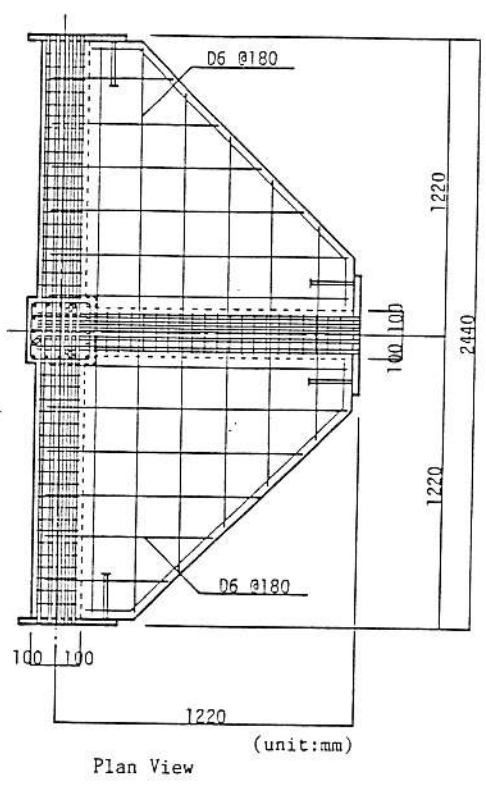
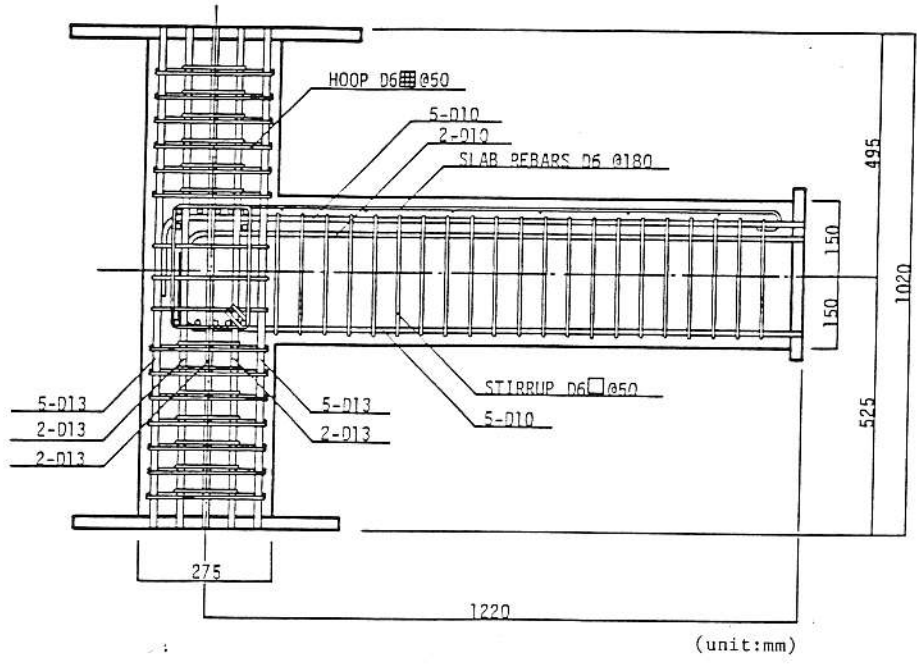
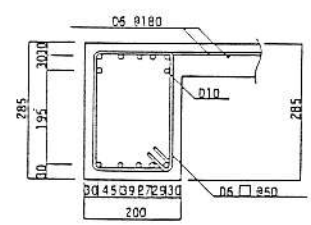


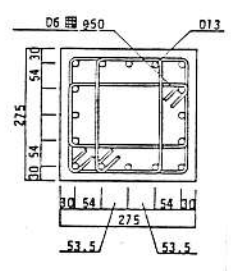
Fig.1(Cont'd): Reinforcement Details of Specimen K2



Longitudinal Beam

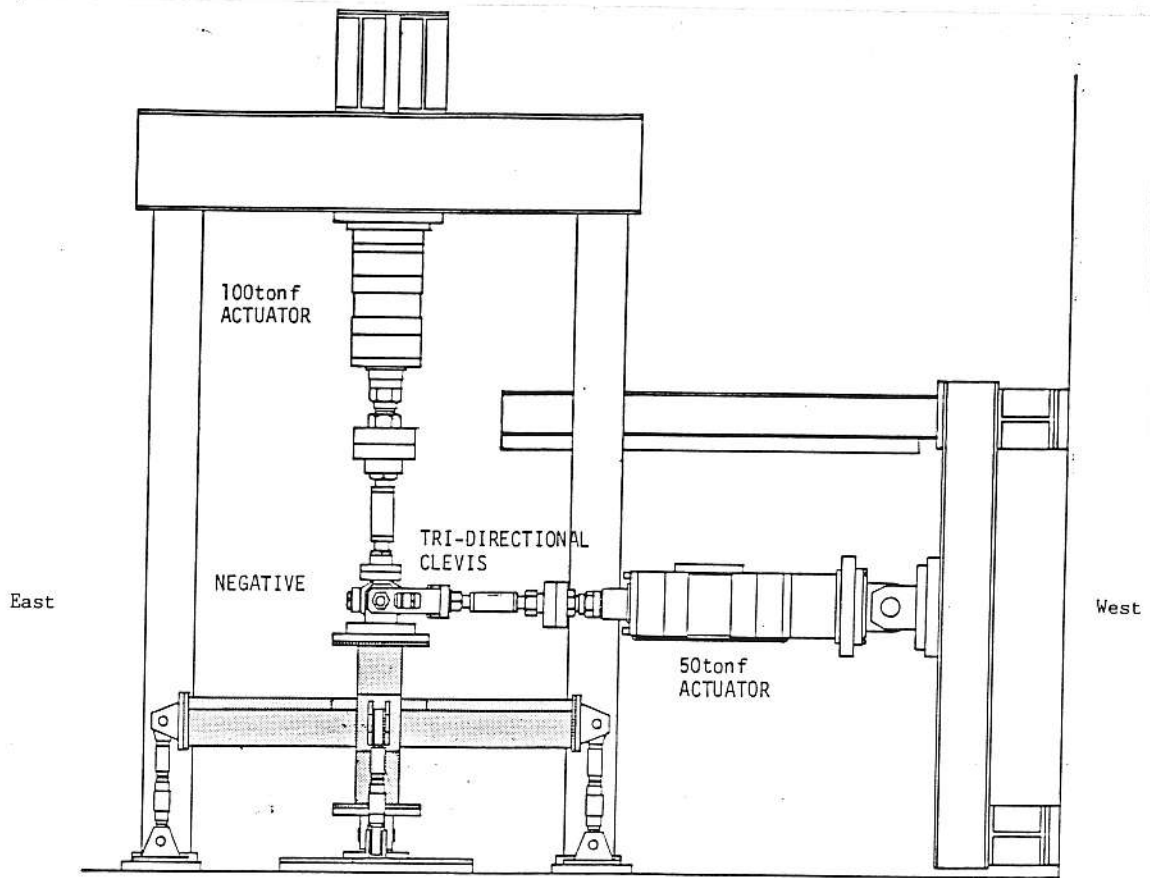


Transverse Beam

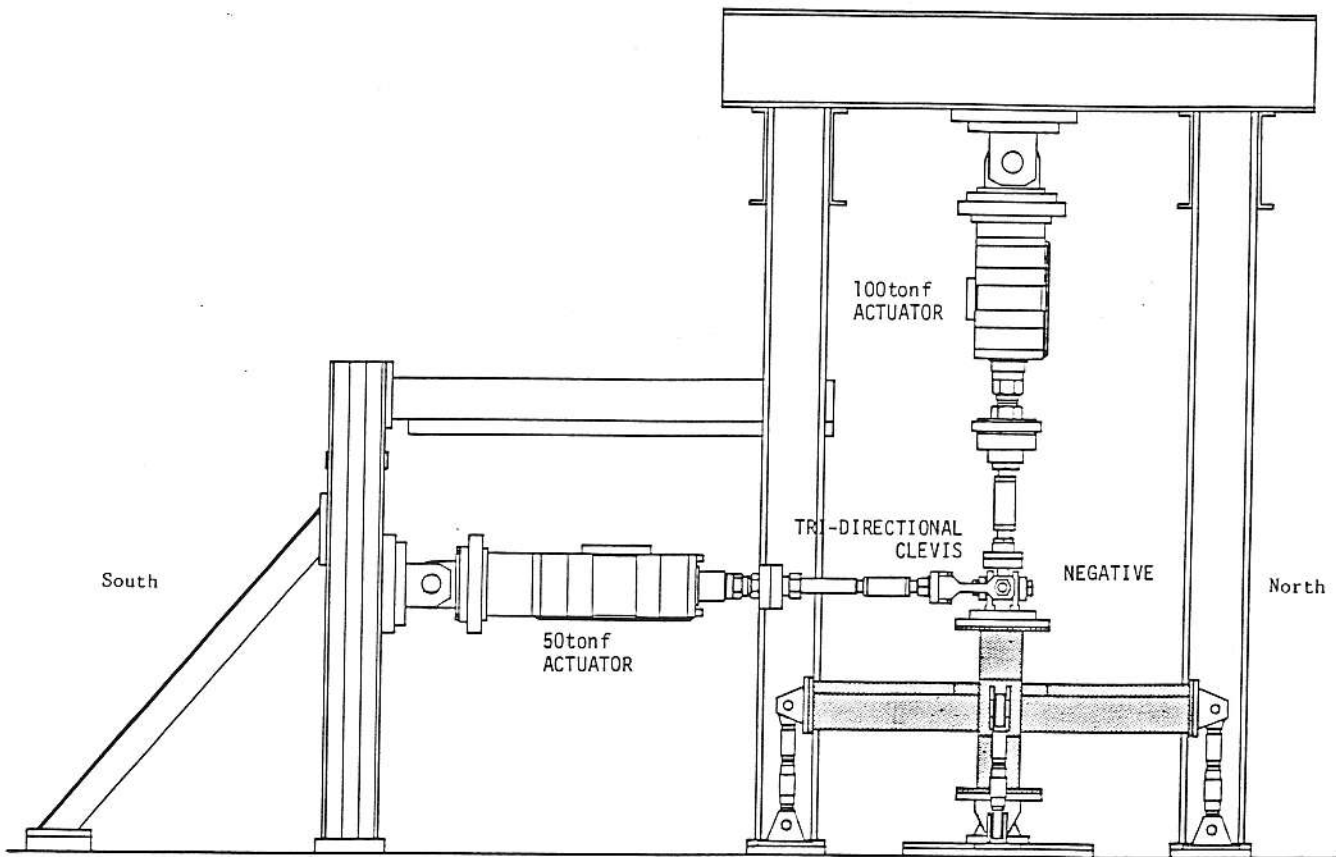


Column

Fig.1(Cont'd): Reinforcement Details of Specimen K3



(a) East-West Direction



(b) South-North Direction

Fig.2: Loading Apparatus

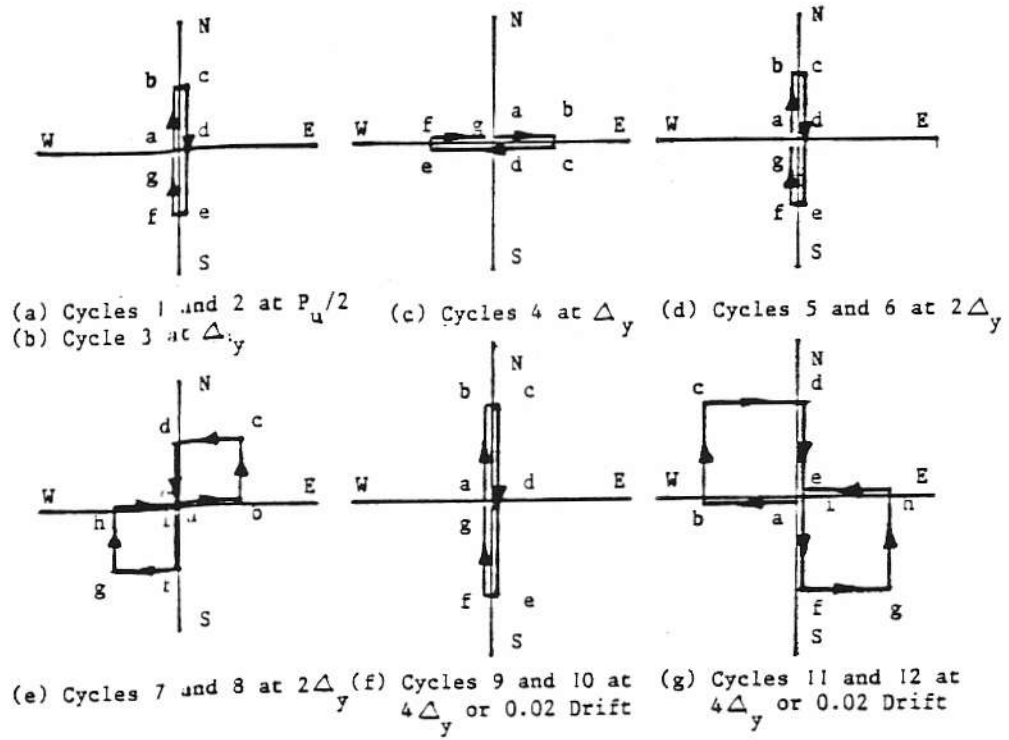
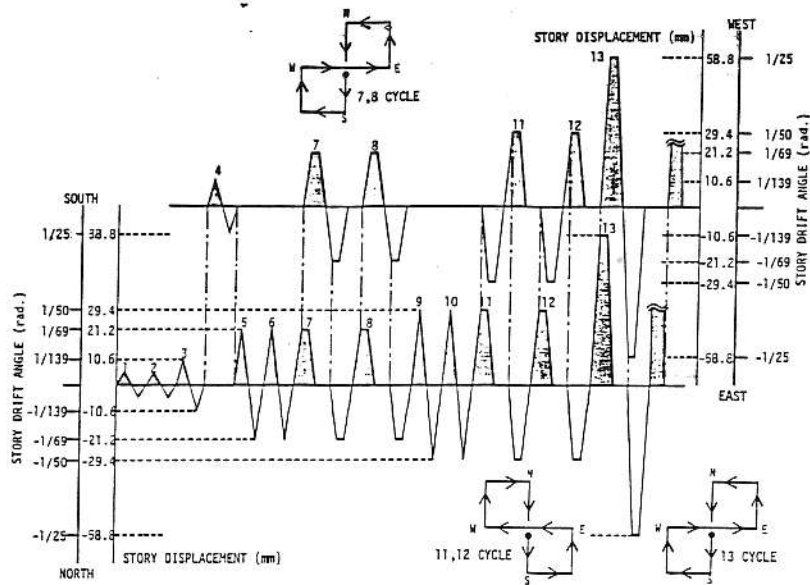
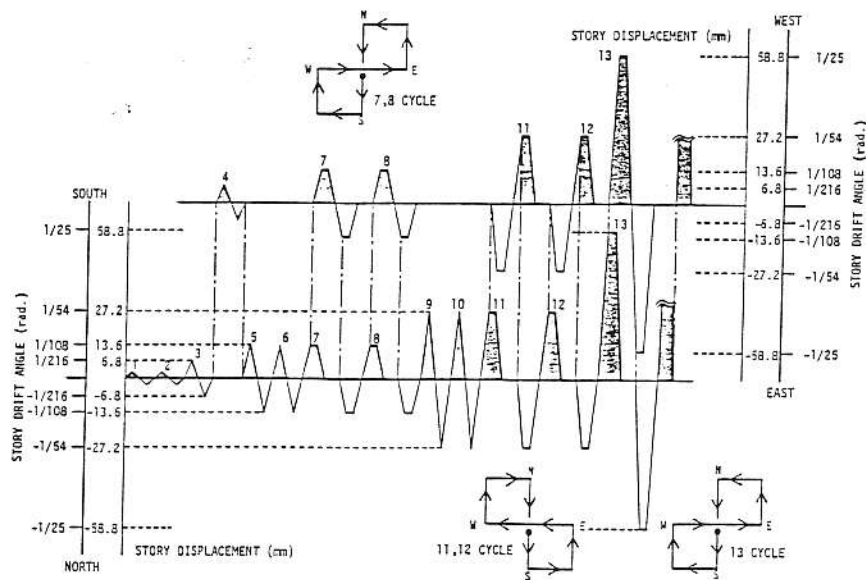


Fig.3: Story Displacement Path of Loading

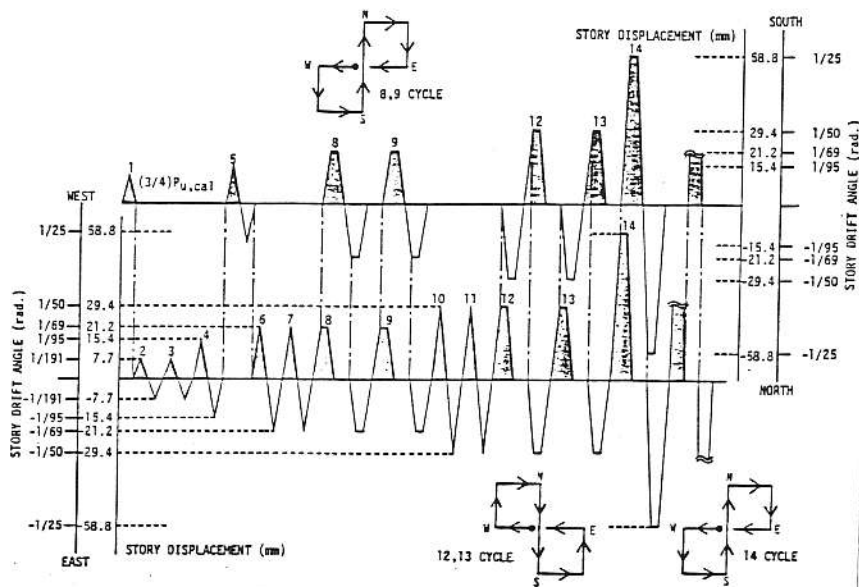




(a) Specimen K1



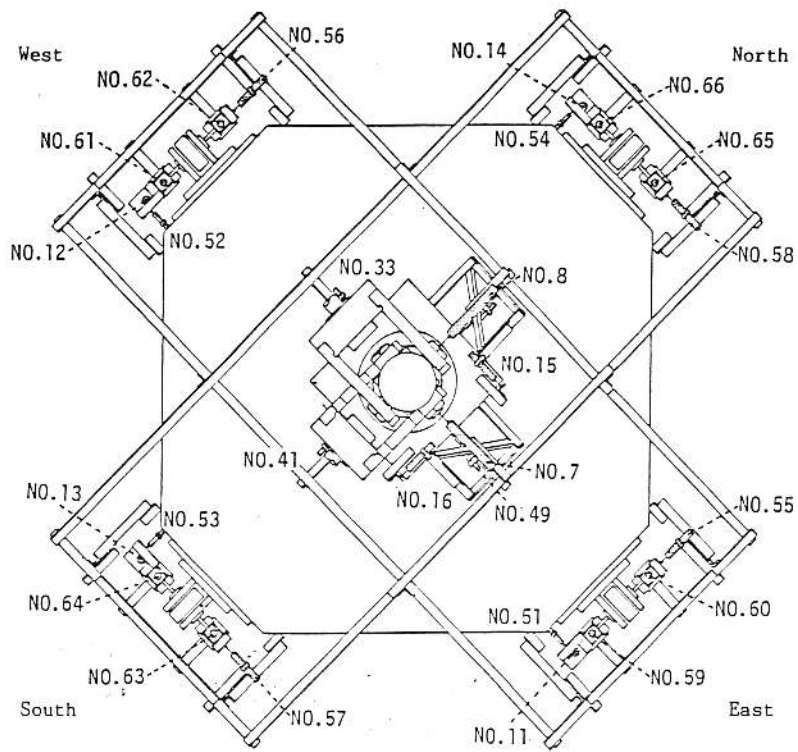
(b) Specimen K2



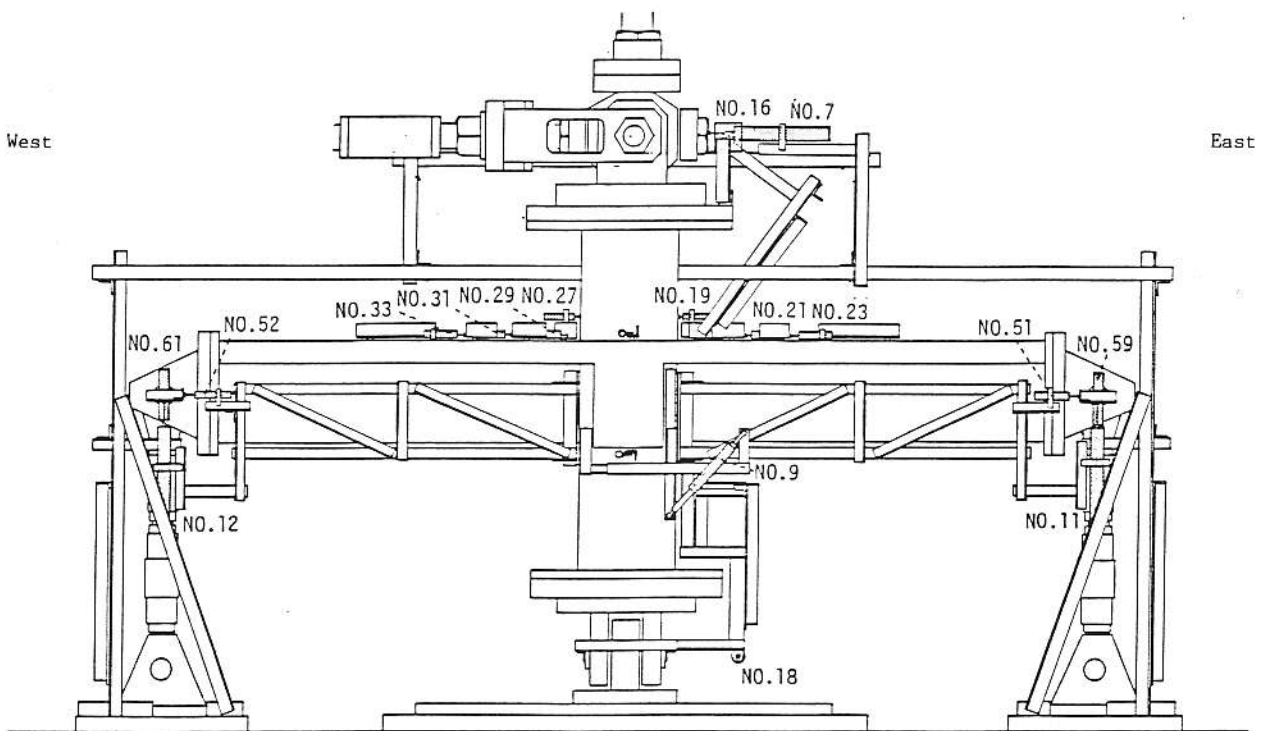
(c) Specimen K3

Fig.4: Actual Story Drift History

*observed*

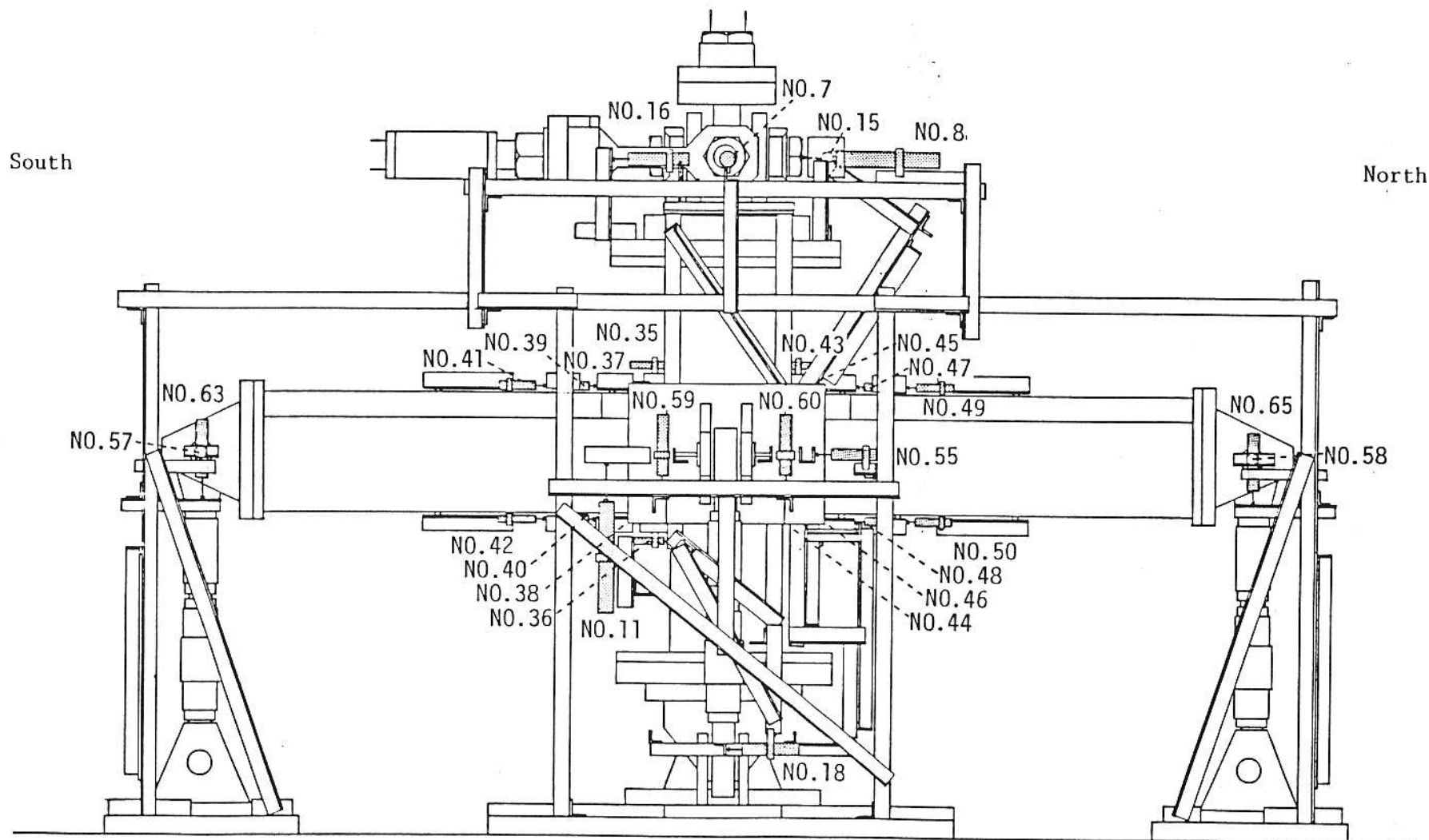


(a) Plan View



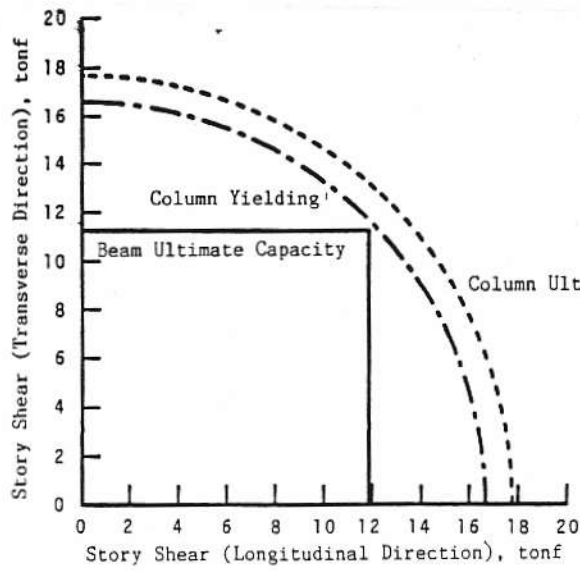
(b) East-West Section

Fig.5: Instrumentation System

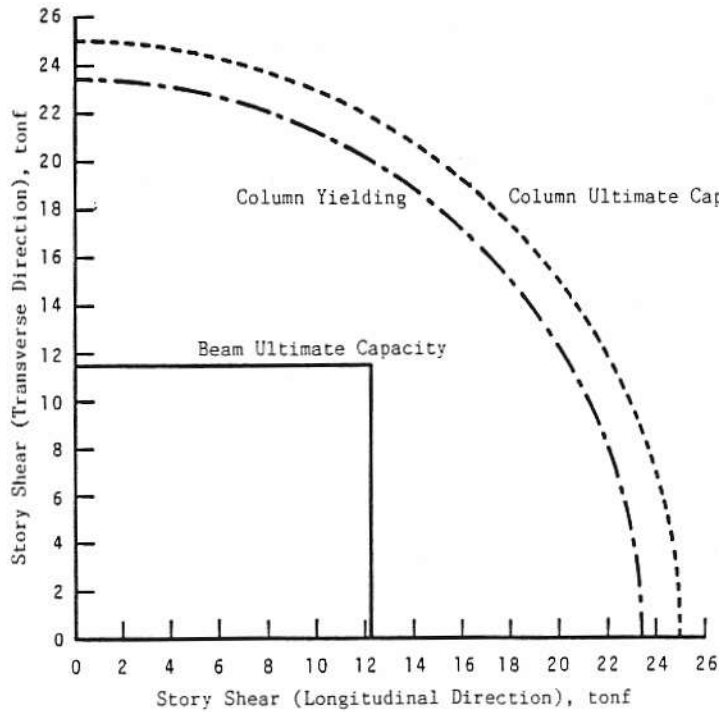


(c) East Elevation

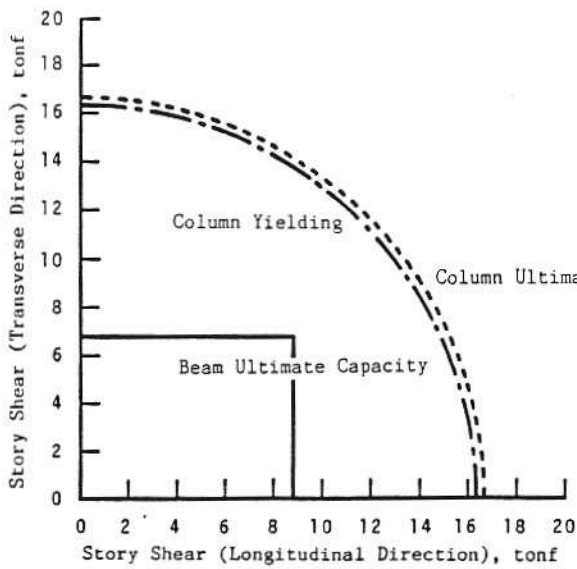
Fig.5(Cont'd): Instrumentation System



(a) Specimen K1



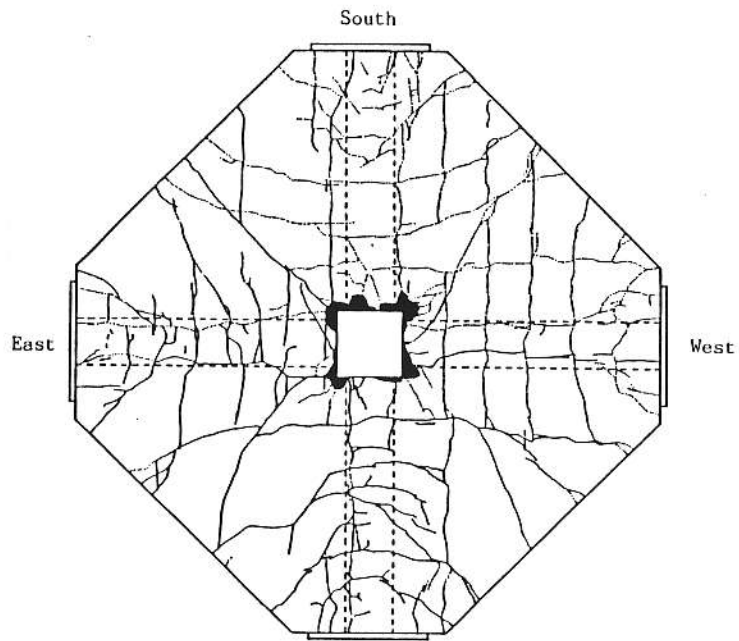
(b) Specimen K2



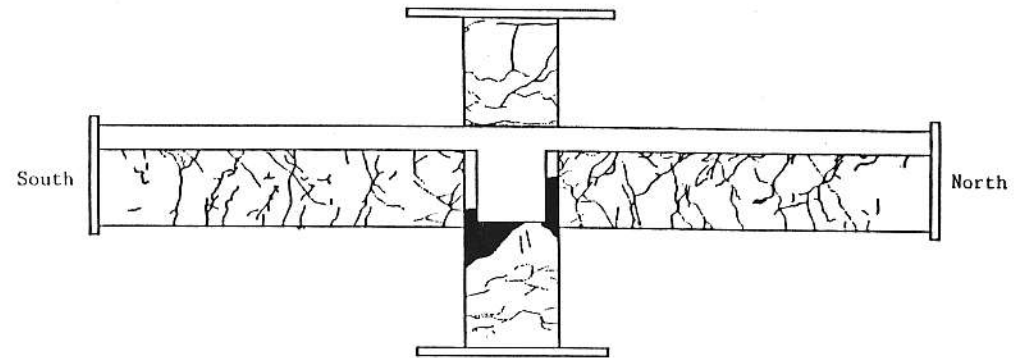
(c) Specimen K3

Fig.6: Calculated Story Shear Capacity by Beam and Column

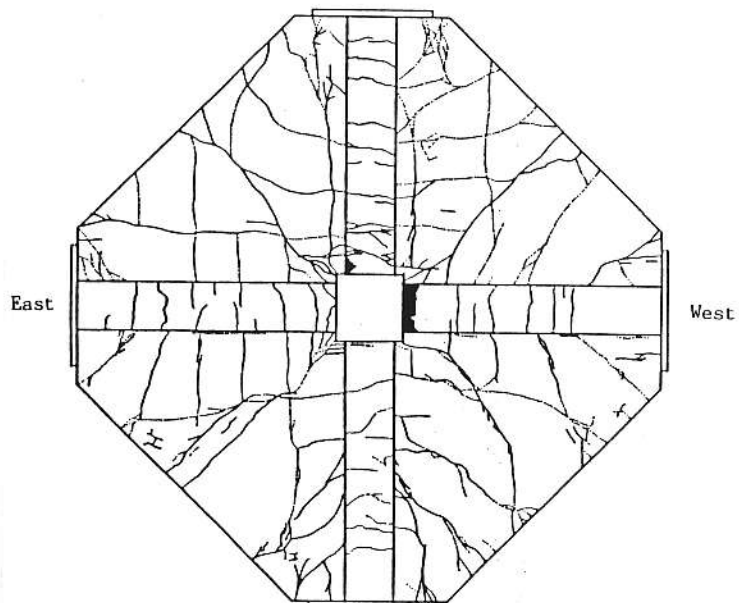
*controlled*



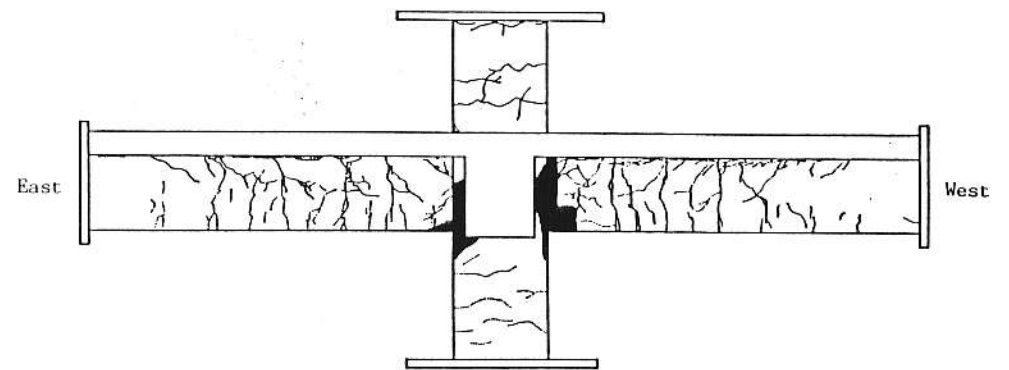
(i) Top View



(i) North - South Direction

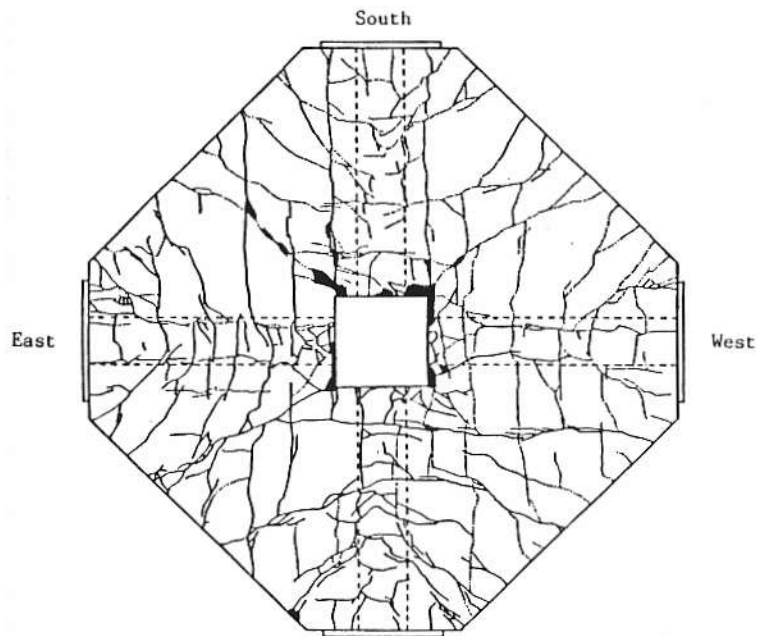


(ii) Bottom View

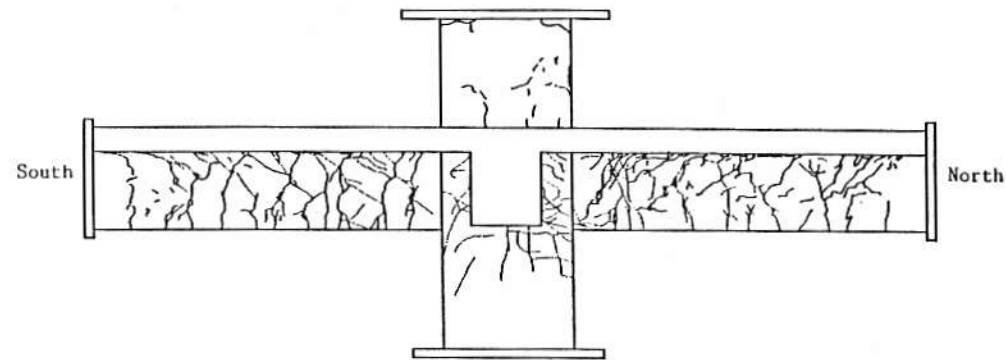


(ii) East - West Direction

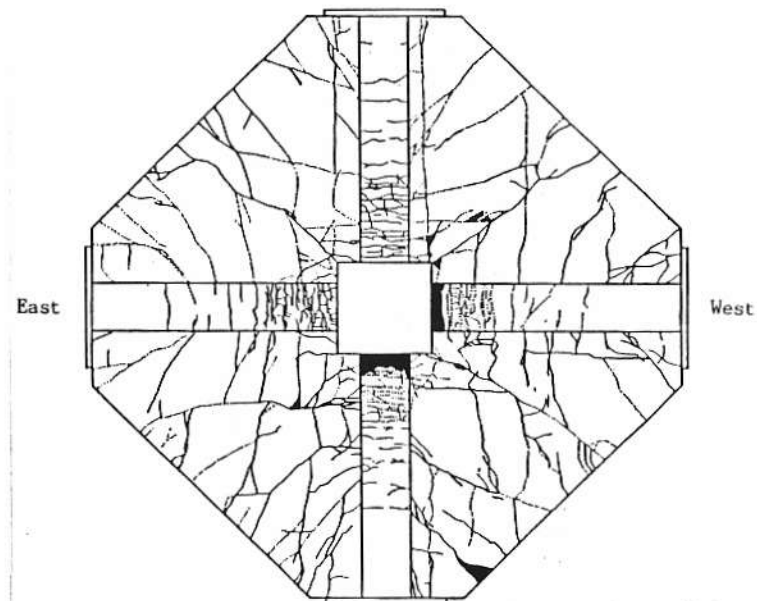
Fig.7: Crack Patterns after Test of Specimen K1



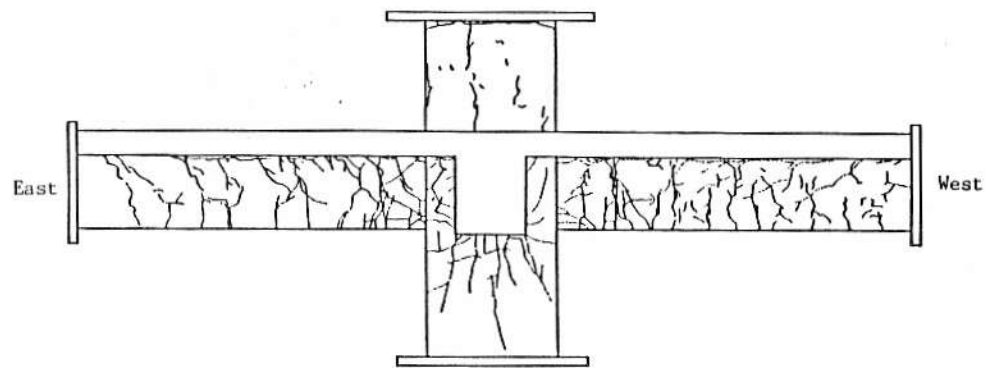
(i) Top View



(i) North - South Direction



(ii) Bottom View



(ii) East - West Direction

Fig.7(Cont'd): Crack Patterns after Test of Specimen K2

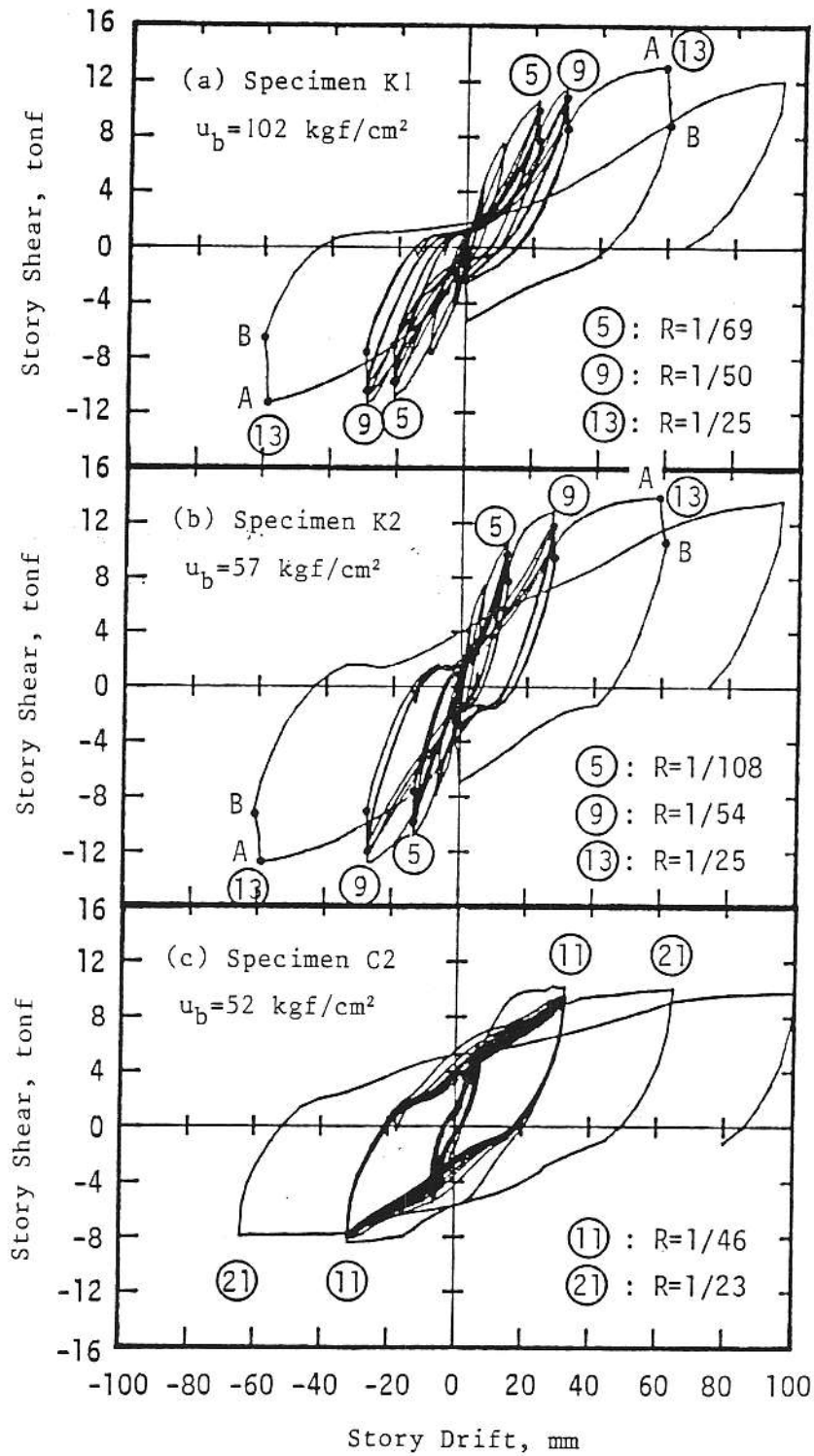


Fig.8: Story Shear-Story Drift Relations

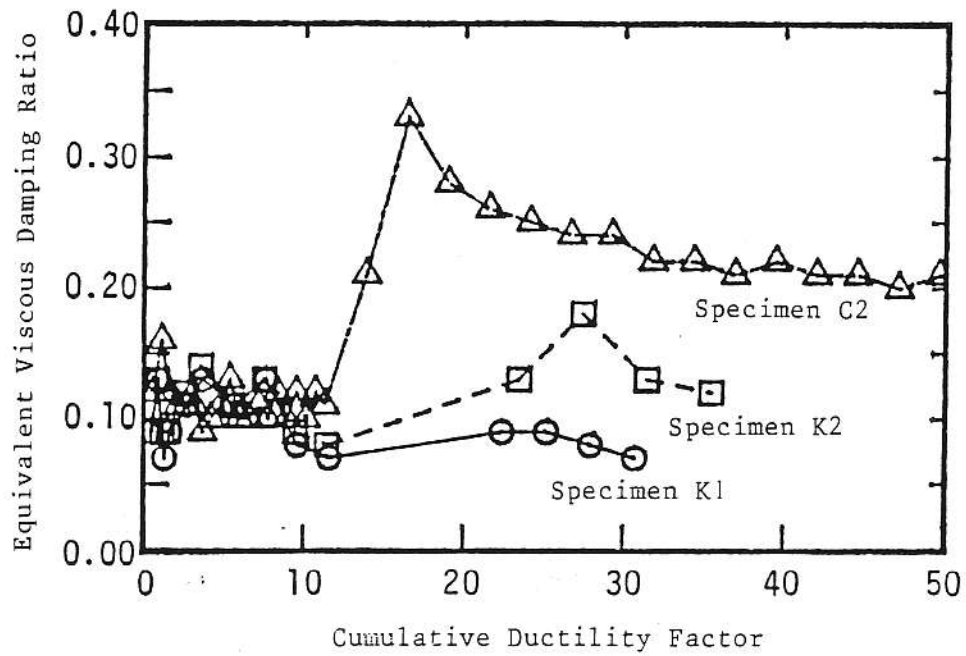


Fig.9: Equivalent Viscous Damping Ratio

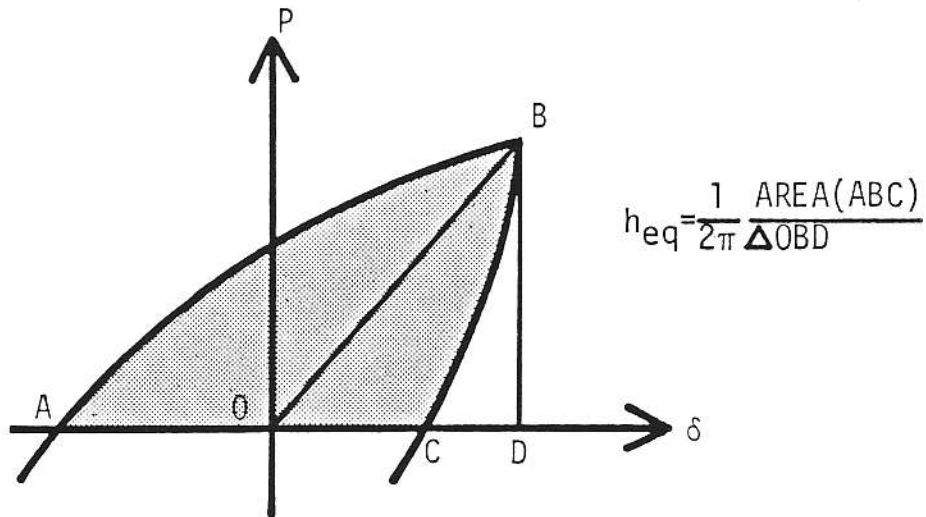
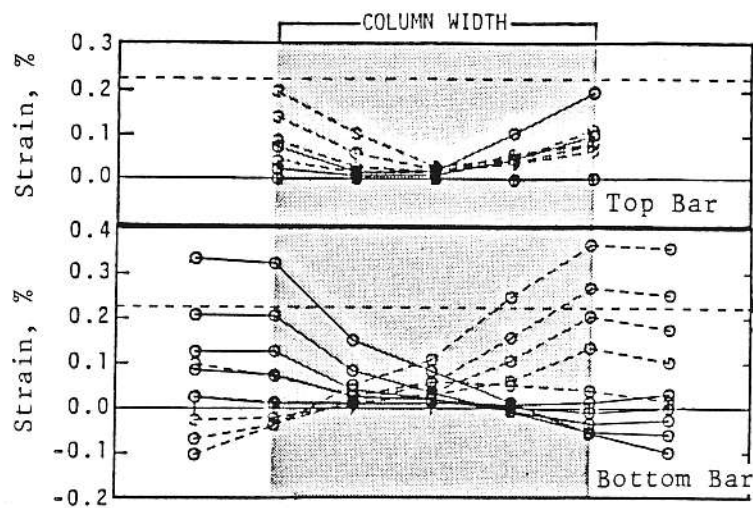
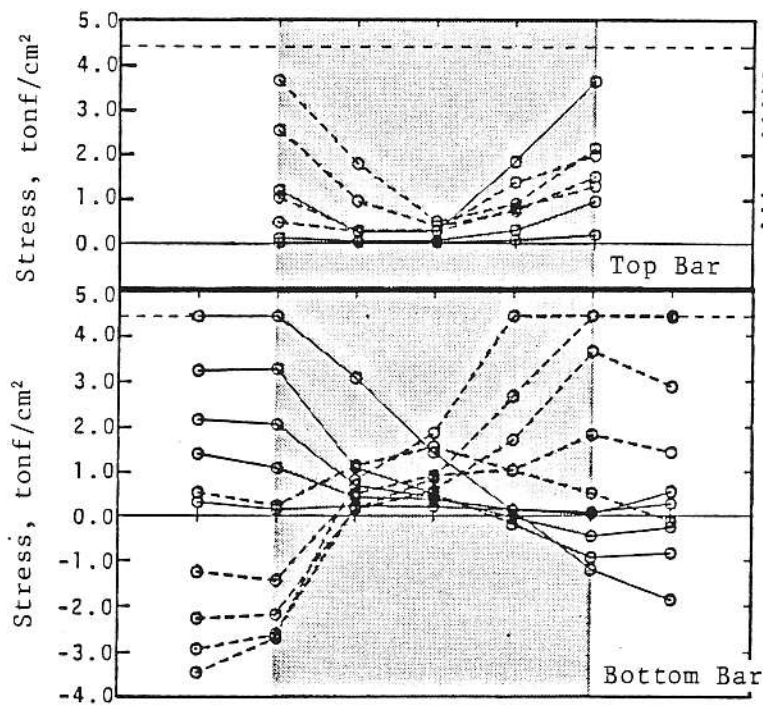


Fig.10: Definition of Equivalent Viscous Damping Ratio





(a) Strain Distribution



(b) Stress Distribution

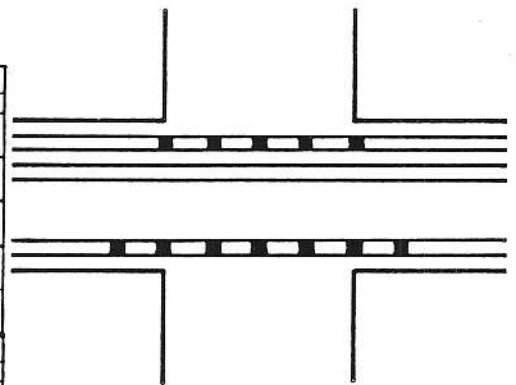


Fig.11: Strain and Stress Distribution along Beam Bar

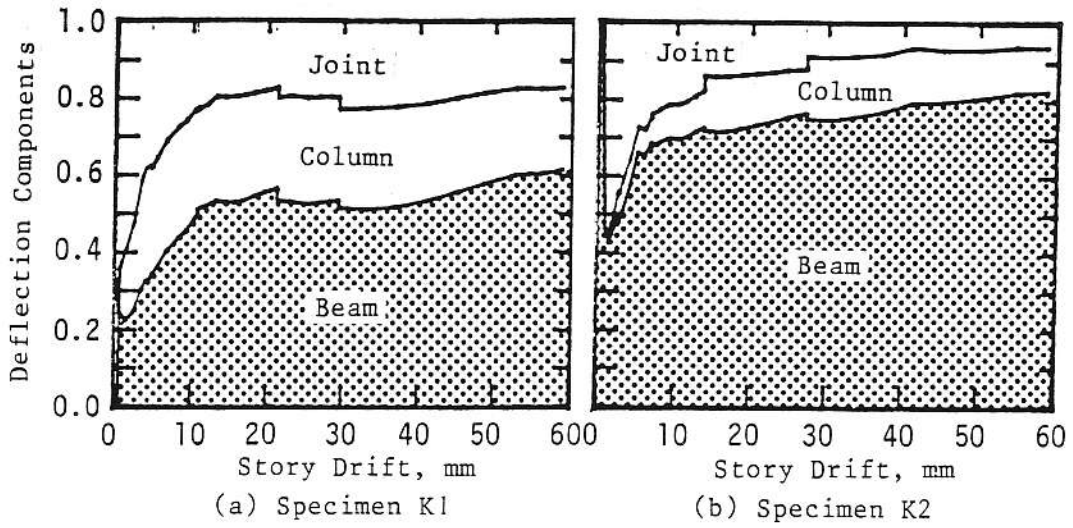


Fig.12: Deflection Components of Story Drift

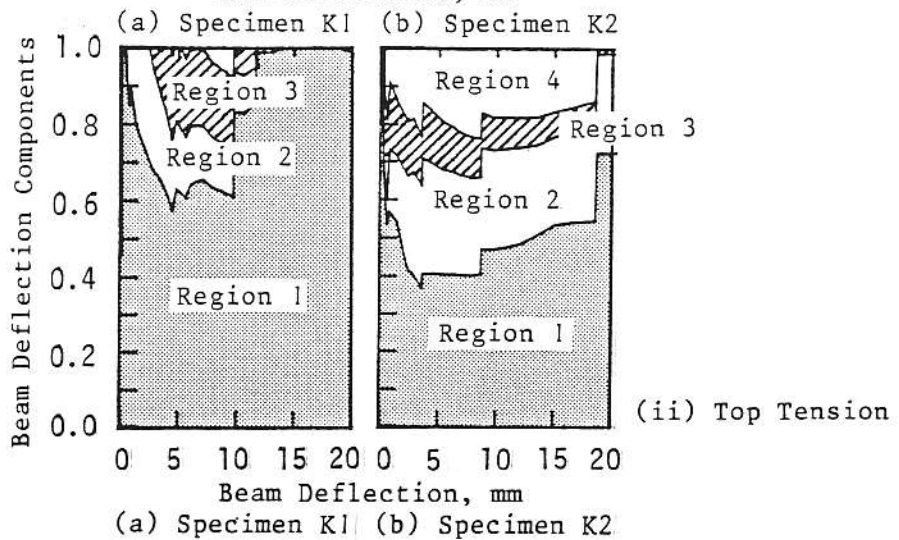
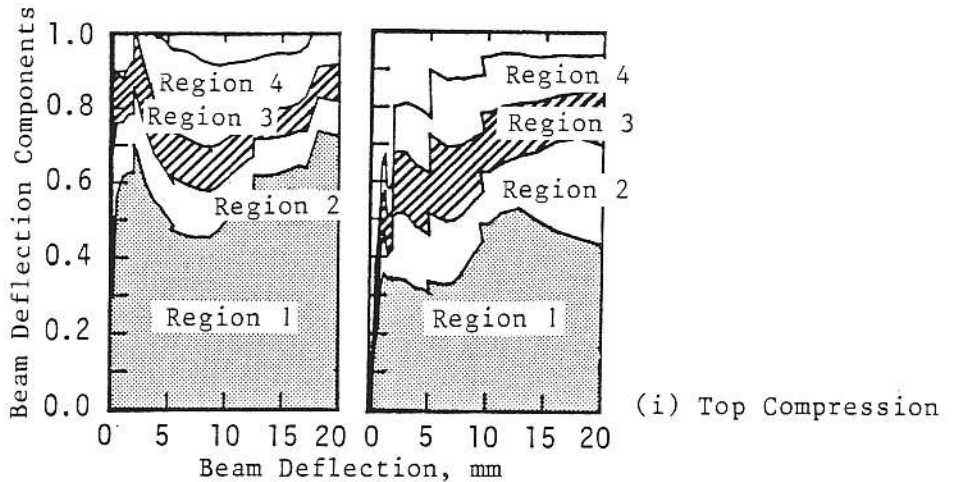
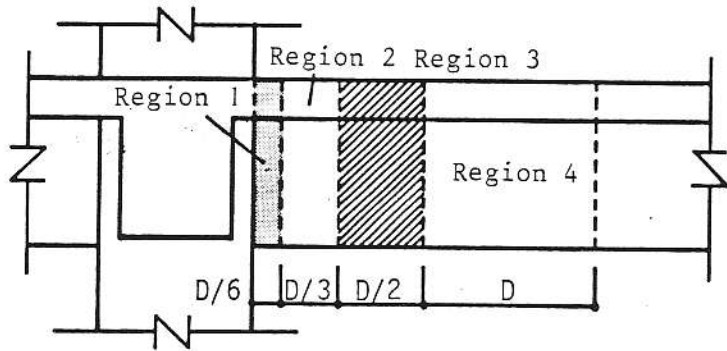
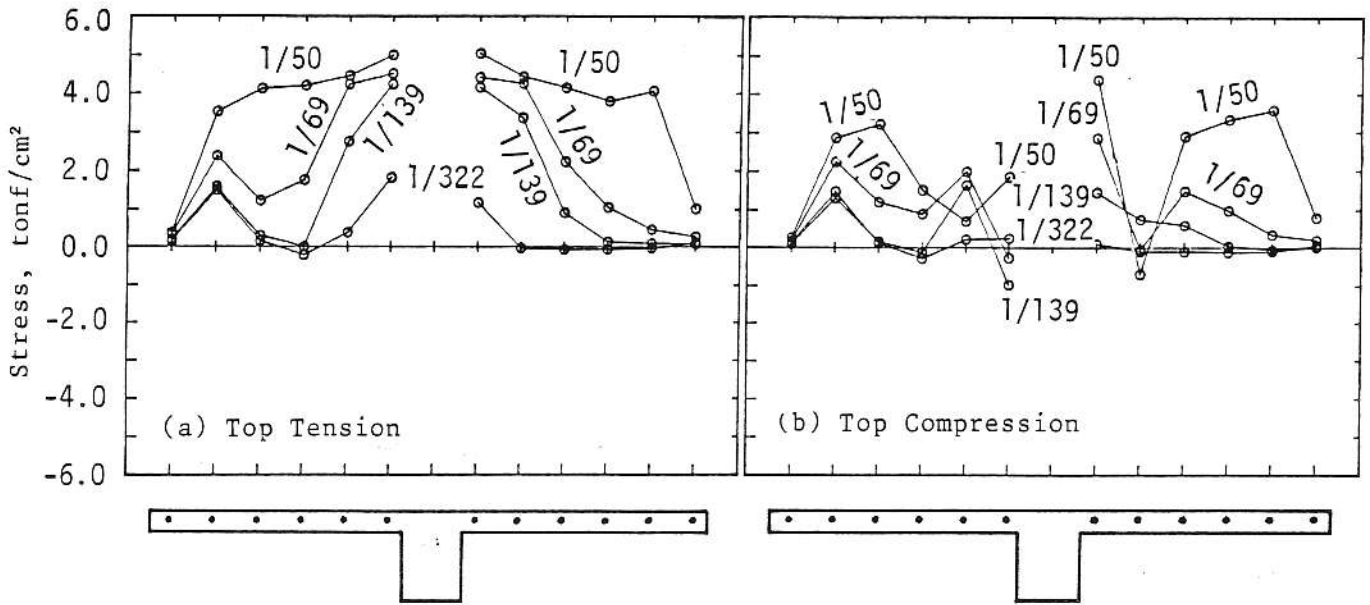
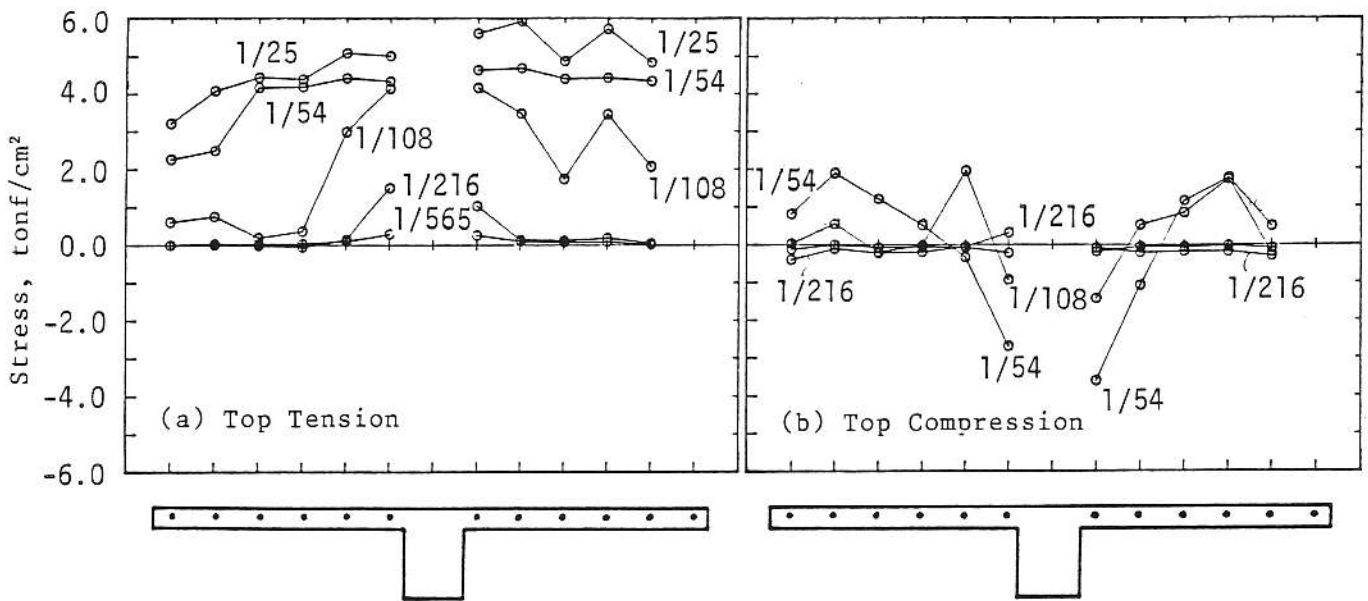


Fig.13: Contribution of Local Rotation to Beam Deflection



(a) Specimen K1



(b) Specimen K2

Fig.14: Stress Distributions of Slab Bars

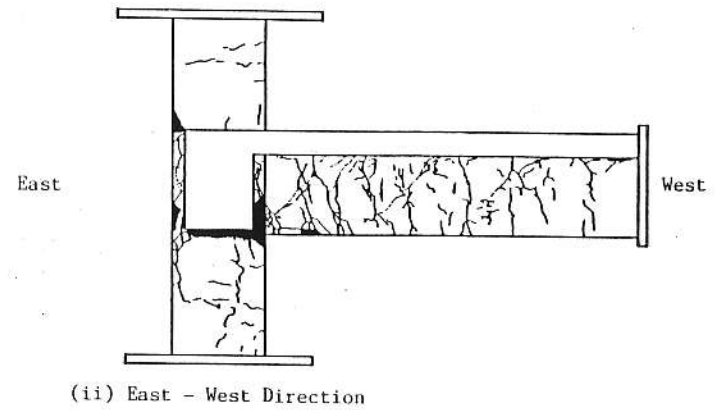
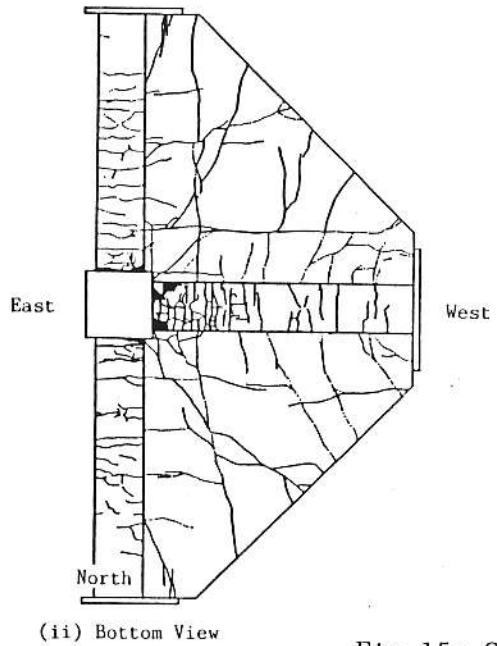
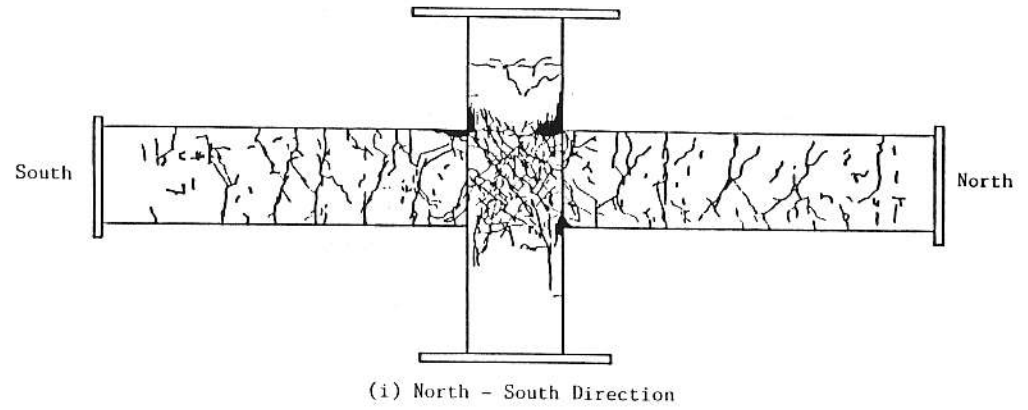
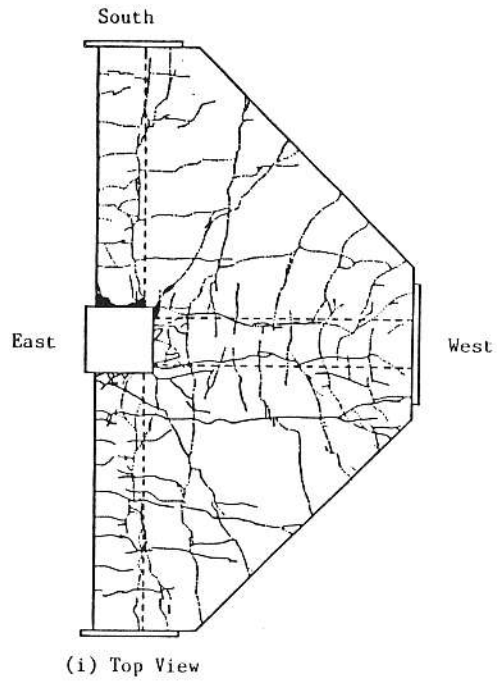


Fig.15: Crack Patterns after Test of Specimen K3

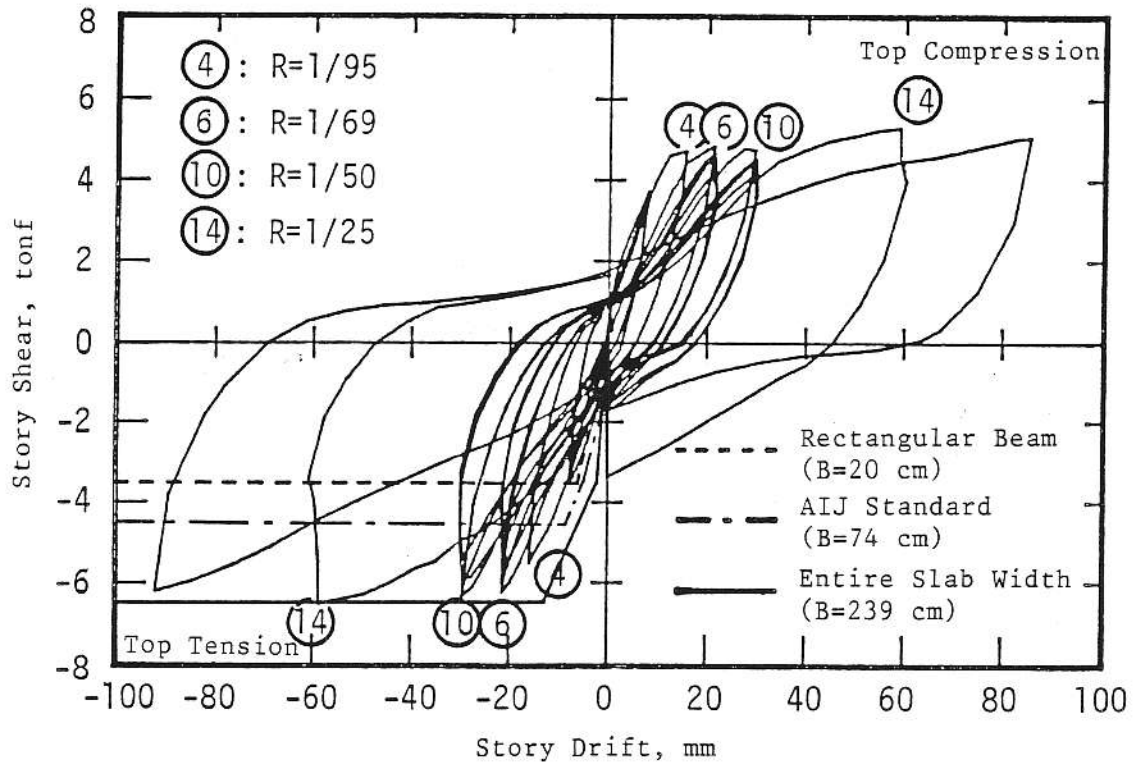
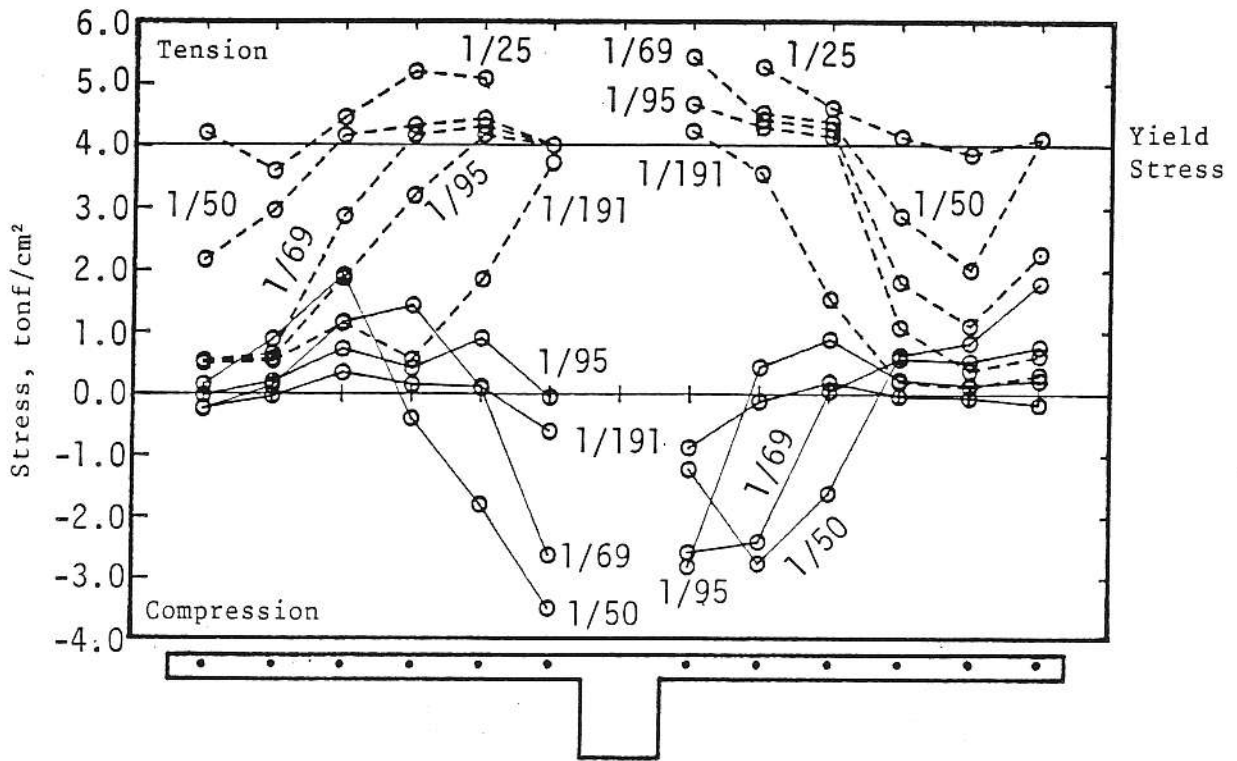
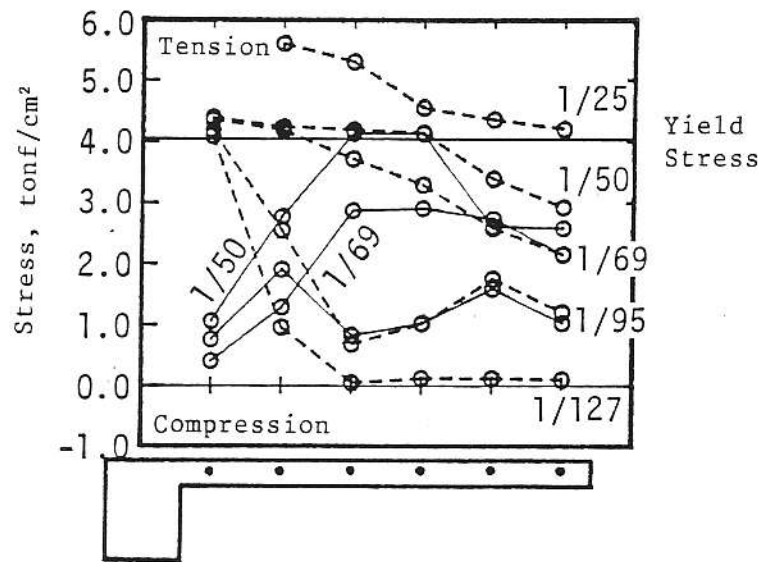
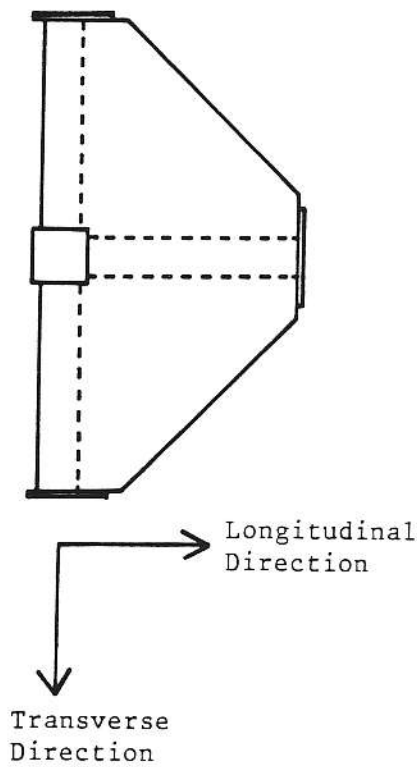


Fig.16: Story Shear-Story Drift Relation in Longitudinal Direction  
 (B: Width of T-section)



(a) Longitudinal Direction



(b) Transverse Direction

Fig.17: Stress Distributions of Slab Bars

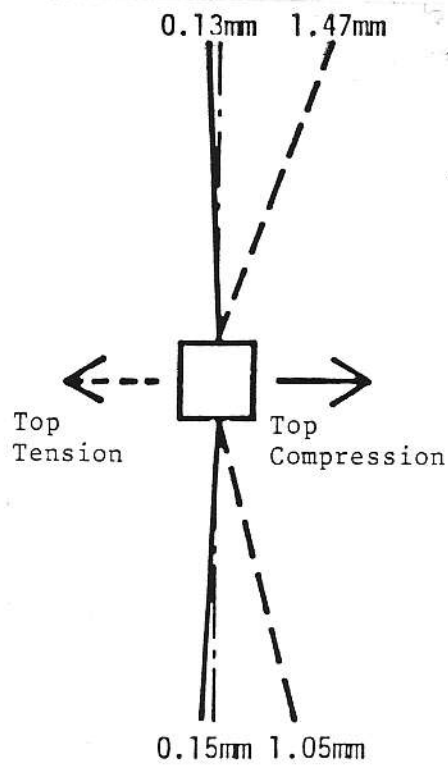


Fig.18: Horizontal Deflection of Transverse Beams

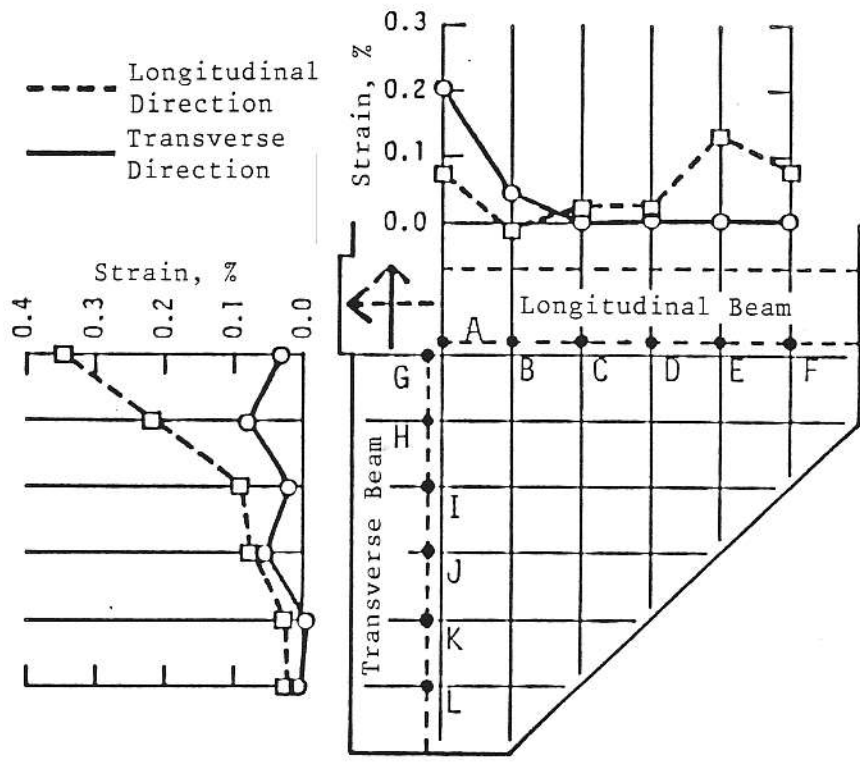


Fig.19: Strain Distribution of Slab Bars

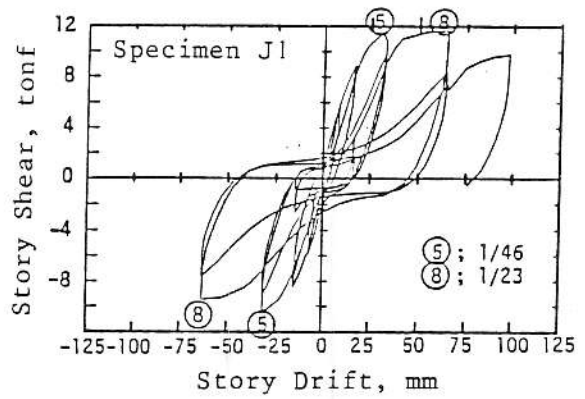
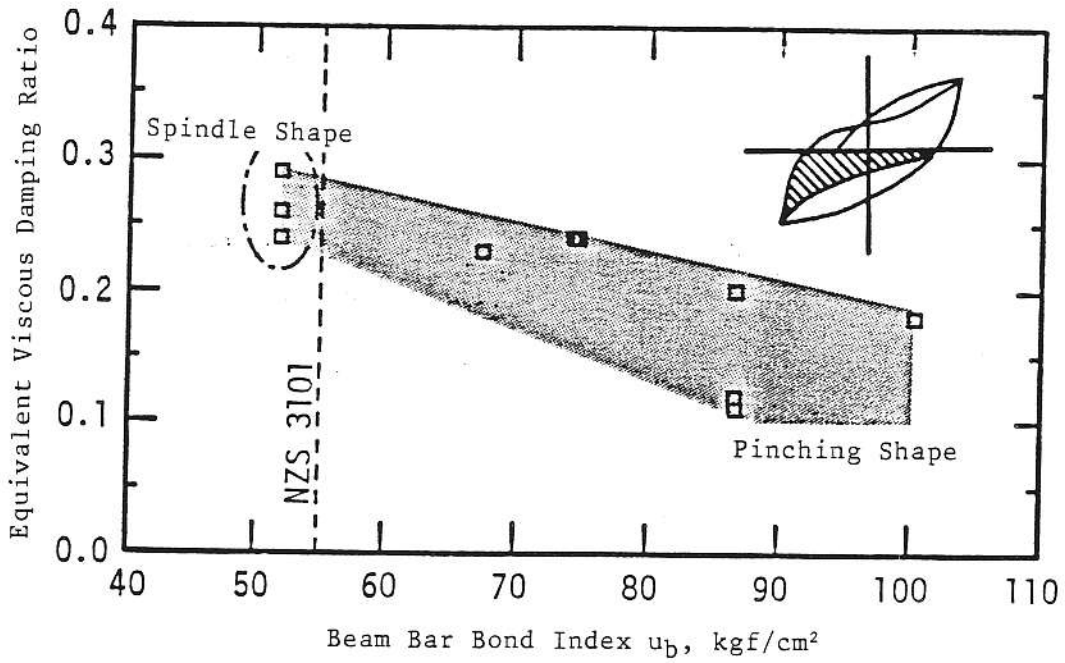
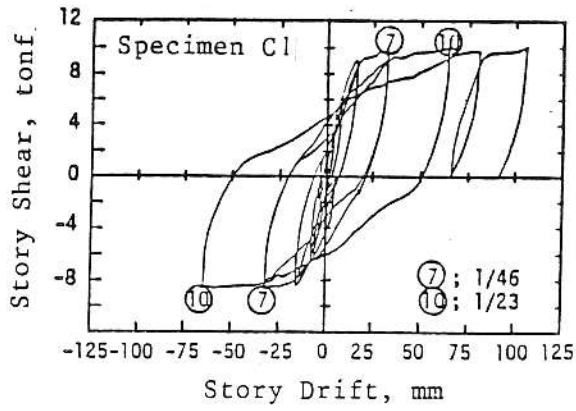


Fig.20: Equivalent Viscous Damping Ratio-Beam Bar Bond Index  $u_b$  Relations